Reduced availability of Nav channels by depolarization or block by TTX boosts burst firing and catecholamine release in mouse chromaffin cells

David H.F. Vandael[1†], Matteo M. Ottaviani[1], Christian Legros[2], Claudie Lefort[2], Nathalie C. Guérineau[2], Arianna Allio[1], Valentina Carabelli[1], Emilio Carbone[1§]

[1]*Department of Drug Science, Laboratory of Cellular and Molecular Neuroscience, N.I.S. Center, CNISM Unit, 10125 Torino, Italy*
[2]*CNRS UMR6214, Inserm U1083, Laboratory of Integrated Neurovascular and mitochondrial Biology, 49045 Angers, France*

Running title: Burst firing in chromaffin cells

Keywords: ion channels, burst firing, chromaffin cells

Number of words in text: 10.043

§ *Corresponding author:* Department of Drug Science
Corso Raffaello 30
10125 - Torino, Italy

phone: +39.011.670.8489
e-mail: emilio.carbone@unito.it

† *Present address*: Institute of Science and Technology Austria
Am Campus 1
A – 3400 Klosterneuburg, Austria

phone: +43.2243.9000.3701
e-mail: david.vandael@ist.ac.at

- **Key points**

- Mouse chromaffin cells (MCCs) of the adrenal medulla possess fast-inactivating Nav channels whose availability alters spontaneous action potential firing patterns and the Ca^{2+}-dependent secretion of catecholamines.
- Here we report that MCCs express large densities of neuronal fast-inactivating Nav1.3 and Nav1.7 channels that carry little or no subthreshold pacemaker currents and can be slowly inactivated by 50% upon slight membrane depolarizations.
- Reducing Nav1.3/Nav1.7 availability by TTX or by sustained depolarization near rest leads to a switch from tonic into burst firing patterns that give rise to elevated Ca^{2+}-influx and increased catecholamine release.
- Spontaneous burst firing is also evident in a small percentage of control MCCs.
- Our results establish that burst firing is an intrinsic firing mode of MCCs that boosts their output, particularly when Nav channel availability is reduced by sustained splanchnic nerve stimulation or prolonged cell depolarizations induced by acidosis, hyperkalemia and increased muscarine levels.

Abstract

Action potential (AP) firing in mouse chromaffin cells (MCCs) is mainly sustained by Cav1.3 L-type channels that drive BK and SK currents and regulate the pacemaking cycle. As secretory units, CCs optimally recruit Ca^{2+} channels when stimulated, a process potentially dependent on the modulation of the AP waveform. Our previous work has shown that a critical determinant of AP shape is Nav channel availability. Here, we studied the contribution of Nav channels to firing patterns and AP shapes at rest (-50 mV) and upon stimulation (-40 mV). Using qRT-PCR and immunoblotting we show that MCCs mainly express TTX-sensitive, fast-inactivating Nav1.3 and Nav1.7 channels that carry little or no Na^+ current during slow ramp depolarizations. Time constants and percentage of recovery from fast inactivation and slow entry into closed-state inactivation are similar to that of brain Nav1.3 and Nav1.7 channels. The fraction of available Nav channels is reduced by half following 10 mV depolarization from -50 to -40 mV. This leads to low amplitude spikes and reductions in repolarizing K^+ currents inverting the net current from outward to inward during the after-hyperpolarization. When Nav channel availability is reduced up to 20% of total either by TTX block or steady depolarization, a switch from tonic into burst firing is observed. The spontaneous occurrence of high frequency bursts is rare in control conditions (14% of cells) but leads to major Ca^{2+}-entry and increased catecholamine release. Thus, Nav1.3/Nav1.7 channel availability sets the AP shape, burst firing initiation and regulates catecholamine secretion in MCCs. Nav channel inactivation becomes important during periods of high activity, mimicking stress responses.

Abbreviations AHP after-hyperpolarization; AP, action potential; BCC, bovine chromaffin cell; CC, chromaffin cells; ISI, interspike interval; LTCC, L-type calcium channel; MCC, mouse chromaffin cell; RCC, rat chromaffin cell

Introduction

Chromaffin cells (CCs) of the adrenal medulla represent the main hub of the sympathetic nervous system. Upon splanchnic nerve stimulation they secrete catecholamines that are central players of the stress response (de Diego *et al.*, 2008; Guerineau *et al.*, 2012). To exert their function, CCs are endowed with a broad array of ion channels that support action potential (AP) generation in a spontaneous manner (Vandael *et al.*, 2010). Upon splanchnic nerve discharge, acetylcholine leads to sustained cell depolarizations, that increase the firing frequency, Ca^{2+}-entry and exocytosis of catecholamine-containing vesicles (Garcia *et al.*, 2006).

Recent studies have shown the importance of Cav1.3 L-type Ca^{2+}-channels (LTCCs) in driving spontaneous firing in mouse chromaffin cells (MCCs) (Marcantoni *et al.*, 2007; Marcantoni *et al.*, 2010). Nevertheless, reports suggesting a partial contribution of voltage-gated Na^+ channels (Nav) to CCs excitability can be found. Early studies showed the existence of a background sodium conductance that could drive Na^+-influx at rest in rat and gerbil CCs (Biales *et al.*, 1976; Brandt *et al.*, 1976). TTX application or Na^+ removal from the extracellular medium reduces, but does not block rat CCs firing (Kidokoro & Ritchie, 1980). In MCCs, Nav channel block by TTX preserves AP firing (Nassar-Gentina *et al.*, 1988), suggesting that Nav channels play a different role in excitability than LTCCs (Vandael *et al.*, 2010). Furthermore, Nav channels in MCCs activate at 24 mV more positive potentials than Cav1.3, suggesting a minor contribution to sub-threshold pacemaker currents (Mahapatra *et al.*, 2011). As in most neurons, Nav channels are shown to be critical for shaping the AP waveform in MCCs (Vandael *et al.*, 2012). Subtle changes in spike shape can lead to drastic changes in Ca^{2+} channel recruitment and in AP-induced Ca^{2+} transients (Li *et al.*, 2007). AP broadening is indeed a common way to optimize presynaptic Ca^{2+} influx at central presynaptic terminals (Engel & Jonas, 2005).

Presently, Nav1.7 is thought to be the main voltage-gated Nav channel expressed in bovine and human adrenal tissues (Klugbauer *et al.*, 1995; Sangameswaran *et al.*, 1997). In the rat adrenal gland, mRNA encoding Nav1.7 is expressed only in the medulla (Morinville *et al.*, 2007), with a plausible localization in CCs, as also reported in PC12 cells (Toledo-Aral *et al.*, 1997). The few functional studies on CC Nav channels show that they are TTX-sensitive, fast-inactivating and rather insensitive to closed-state inactivation (Fenwick *et al.*, 1982; Lou *et al.*, 2003; Wada *et al.*, 2008; Mahapatra *et al.*, 2011). The contribution of Nav channels to CC spiking at rest and upon stimulation remains controversial and studies that considered Nav properties and availability at physiologically relevant potentials (-55 to -40 mV) are lacking.

Here, using qRT-PCR and western-blot analysis we show that besides Nav1.7, Nav1.3 is highly expressed together with β1-3 subunits. The two principal MCC Nav channels possess rather similar activation-inactivation properties (Catterall *et al.*, 2005) and contribute to spike generation but not to the pacemaker current. This is evident when both channels are blocked by TTX or when their availability is strongly reduced by steady inactivation during slight membrane

depolarizations. Block or reduced Nav1.3/Nav1.7 availability induces a switch of firing from tonic single APs to doublet and triplet bursts of APs which cause a paradoxical increase of Ca^{2+}-entry and catecholamine secretion. Nav channel inactivation thus seems to be an important phenomenon that boosts MCC output during strong splanchnic nerve discharges as occurs during the stress-response (Garcia *et al.*, 2006) or during prolonged depolarizations near rest induced by acidosis, hyperkalemia or increased muscarine levels.

Methods

Ethical approval - Ethical approval was obtained for all experimental protocols from the University of Torino Animal Care and Use Committee, Torino, Italy. All experiments were conducted in accordance with the National Guide for the Care and Use of Laboratory Animals adopted by the Italian Ministry of Health. Every effort was made to minimize animal suffering and the number of animals used. For removal of tissues, animals were deeply anaesthetized with CO2 inhalation and rapidly killed by cervical dislocation.

Cell culture - Chromaffin cells were obtained from male C57BL/6J mice (Harlan, Correzzano, Italy) of 3 months. Animals were killed by cervical dislocation, all procedures were performed according to the guidelines established by the National Council on Animal Care and were approved by the local Animal Care committee of the University of Turin. Under sterile conditions the abdomen was opened, the adrenal glands were isolated, and transferred to an ice cold Ca^{2+} and Mg^{2+} free Locke's buffer containing (in mM) 154 NaCl, 3.6 KCl, 5.6 $NaHCO_3$, 5.6 glucose and 10 HEPES, pH 7.4 (Marcantoni *et al.*, 2009; Vandael *et al.*, 2012). Under a dissecting microscope the adrenal glands were decapsulated and subsequently subjected to an enzymatic dissociation with 20-25 units/ml papain (Worthington Biochemical Corporation, Segrate, Italy) dissolved in DMEM (GIBCO, Invitrogen Life Technologies, Monza, Italy) supplemented with 1.5 mM of L-cysteine, 1 mM of $CaCl_2$ and 0.5 mM of EDTA (Sigma Aldrich, Munich, Germany) for 25 -30 minutes at 37°C in a water saturated atmosphere with 5% CO_2. Afterwards, two washing steps were performed with DMEM supplemented with 1mM $CaCl_2$ and 10 mg/ml of BSA (Sigma Aldrich). Adrenal medulla's were re-suspended in DMEM containing 1% pen/strep and 15% fetal bovine serum (both from Sigma Aldrich) and were mechanically dissociated with a fire polished Pasteur pipette. A drop (100 µL) of this concentrated cell suspension was plated on poly-ornithine (1mg/ml) and laminin (5 µg/ml) coated petri- dishes and subsequently (30 minutes later) 1.9 ml of DMEM containing 1% pen/strep and 15% fetal bovine serum (all from Sigma Aldrich) was added. The primary chromaffin cell culture was kept in an incubator at 37°C at water saturated atmosphere with 5% CO_2. Measurements were performed on cultured MCCs two to five days after plating.

Electrophysiology - Macroscopic whole-cell currents and APs were recorded in perforated-patch conditions using a multiclamp 700-B amplifier and pClamp 10.0 software (Molecular Devices, Sunnyvale, CA, USA) (Marcantoni *et al.*, 2010; Vandael *et al.*, 2012). Traces were sampled at 10 KHz using a digidata 1440 A acquisition interface (Molecular Devices, Sunnyvale, CA, USA) and filtered using a low-pass Bessel filter set at 1-2 KHz. Borosilicate glass pipettes (Kimble Chase life science, Vineland, NJ, USA) with a resistance of 2-3 MΩ were dipped in an eppendorf tube containing intracellular solution before being back filled with the same solution containing 500µg/ml of amphotericin B (Sigma Aldrich, Munich, Germany), dissolved in DMSO (Sigma Aldrich, Munich, Germany) (Cesetti *et al.*, 2003). Recordings were initiated after amphotericin B lowered the access resistance below 15 MΩ (5-10 min). Series resistance was compensated by 80% and monitored throughout the experiment. Fast capacitive transients during step-wise depolarisations (in voltage-clamp mode) were minimized online by the use of the patch clamp analogue compensation. Uncompensated capacitive currents were further reduced by subtracting the averaged currents in response to P/4 hyperpolarising pulses. To eliminate any additional leakage current, the recorded ion current during step depolarizations was subtracted from traces measured in the presence of saturating concentrations of TTX (300 nM) (Carbone & Lux, 1986). The same was applied for the AP-clamp experiments in which the cell was clamped to a train of previously recorded APs. L-type Ca^{2+}-currents were isolated by subtracting the non L-type current (in the presence of nifedipine, 3 µM) from the whole cell Ca^{2+} current.

Single channel recordings were performed on perforated microvesicles that were pulled out of the cell after amphotericin B lowered the access resistance below 15 MΩ (Levitan & Kramer, 1990). Glass pipettes for this purpose were pulled and fired polished in order to obtain electrode resistances of ~7 MΩ (Carabelli *et al.*, 2001). Single channel recordings were sampled at 20 kHz and low-pass filtered at 2 kHz. Block by TTX at the end of the recording gave rise to single channel-free baseline traces that were averaged and used to correct for the capacitive artefacts. Further baseline correction was performed manually using Clampfit software. Mean open and closed times were analyzed using pClamp software. The criteria for selecting the detection levels of channel opening and closing were similar to those previously described (Carbone & Lux, 1987; Carabelli *et al.*, 2001). The effective minimal duration of detectable opening and closing was set to 150 µs (Carbone & Lux, 1986)

Carbon fibres (5 µm tip diameter) were purchased from Ala Scientific Instruments Inc. (Westbury, NY, USA). Electrochemical recordings were performed using a HEKA EPC-10 amplifier. Amperometric measurements were performed by positioning the carbon fiber microelectrode (polarized at +800 mV) adjacent to the cell membrane (Carabelli *et al.*, 2007b; Marcantoni *et al.*, 2009). MCCs were current clamped and spontaneous firing was suppressed by the injection of -5pA. Subsequently inhibition was relieved and cells were allowed to fire spontaneously for 40 s. Amperometric currents were sampled at 4 kHz and low-pass filtered at 1 kHz. Data were

analysed by IGOR macros (WaveMetrics, Lake Oswego, OR, USA) as described elsewhere (Segura et al. 2000). The analysis of individual exocytotic events was done by measuring the following parameters: maximum oxidation current (I_{max}), spike width at half height ($t_{1/2}$), total charge of the spike (Q), ascending slope of the spike (m) and time to reach the spike (t_p). All experiments were performed at room temperature.

Solutions - Intracellular solution for current-clamp and Na^+ current/K^+ current measurements in voltage clamp or AP-clamp mode was composed of (in mM) 135 KAsp, 8 NaCl, 20 HEPES, 2 $MgCl_2$, 5 EGTA, pH 7.4 (with NaOH; Sigma Aldrich). For Ca^{2+} current recordings the intracellular solution contained (in mM) 135 Cs-$MeSO_3$, 8 NaCl, 2 $MgCl_2$ and 20 HEPES, pH 7,4 (with CsOH; Sigma Aldrich). The extracellular solution used for current-clamp measurements is based on a physiological Tyrode's solution containing in mM: 130 NaCl, 4KCl, 2 $CaCl_2$, 2 $MgCl_2$, 10 HEPES and 10 glucose; pH 7.4 (with NaOH). The same solution was used as well to measure K^+ currents. K_V currents were obtained by application of 200 µM Cd^{2+} while Ca^{2+}-activated BK currents were estimated by subtracting K_V from the total K^+ currents. In RCCs and MCCs, 500 µM Cd^{2+} are shown to be effective as 1 µM paxilline to block transient BK channels (Marcantoni *et al.*, 2007; Marcantoni *et al.*, 2010) and we have proved that in 2 mM extracellular Ca^{2+}, 200 µM Cd^{2+} is as effective as 500 µM Cd^{2+} in blocking Cav channels and Ca^{2+}-activated BK channels (not shown). In addition, residual Cd^{2+}-insensitive voltage-dependent BK currents contribute little (< 5%) to the total BK currents at +20 to +30 mV (Berkefeld & Fakler, 2013). Thus, isolation of transient BK currents using 200 µM Cd^{2+} appears a justified protocol. The extracellular solution used for Na^+ current measurements was composed of (in mM): 104 NaCl, 30 TEACl, 4 KCl, 2 $CaCl_2$, 2 $MgCl_2$, 10 HEPES and 10 glucose, pH 7,4 (with NaOH). The extracellular solution used for Ca^{2+} current measurements in voltage- and AP-clamp configuration contained (in mM): 135 TEA, 2 CaCl, 2 $MgCl_2$, 10 HEPES, 10 glucose, pH 7.4 (with TEA-OH; Sigma Aldrich). TTX was purchased from Tocris Bioscience (Bristol, UK), dissolved in bi-distilled water and stored at -20 °C until used. Solutions were applied using a gravity based perfusion system. Current-clamp data were not corrected for the liquid junction potential (LJP) (15.4 mV at 22°C; see (Marcantoni *et al.*, 2010)) since TTX (up to 1 µM) did not affect the LJP any further.

Real time PCR and western blot - Adrenal medullary tissue was prepared from six mice as already described (Desarmenien *et al.*, 2013). After removal, the glands were incubated in RNAlater® RNA Stabilization Reagent (Sigma-Aldrich, Saint Quentin Fallavier, France) at 0-4°C for 24 h. Then, the glands were decapsulated and the cortical tissue was gently separated, under microscope, from the medulla using micropincers and discarded. Both macrodissected adrenal medulla from each animal were pooled and used separately for RNA or protein extraction. Total RNA was extracted using the RNeasy® micro kit (Qiagen, Courtaboeuf, France). For retrotranscription, total RNA (200 ng) from adrenal medulla of each animal was used and the reactions were performed using random hexamer primers and the QuantiTect Reverse

Transcription kit (Qiagen). Real-time PCR assays were carried out on a LightCycler 480 Instrument II (Roche, Meylan, France) with Sybr® Select Master Mix (Applied Biosystems®). Gene-specific primers for real-time PCR (Table 1) were designed using the Primer3 Software. Differences in transcript level were determined using the cycle threshold method, as described by the manufacturer. Specificity of amplification was checked by melting curve analysis and gene expression was normalized to expression of three housekeeping genes: Gapdh (glyceraldehyde-3-phosphate dehydrogenase), Gusb (beta-glucuronidase) and Hprt (hypoxanthine phosphoribosyltransferase 1), according to the formula $E = 2^{-(Ct(Target)-Ctmean(Reference))}$, where Ct is the threshold cycle. Amplicon sizes (70-106 bp) and AT content (47-55%) were chosen to allow comparison between relative expression values obtained for each gene (Colborn *et al.*, 2008).

For protein extraction, adrenal medullary and brain tissues were dissociated using lysis buffer (10 mM Tris-HCl, pH 7.4, 5 mM EDTA, 1 mM sodium orthovanadate and 10 mM NaF as phosphatase inhibitors, 10 mM β-glycerophosphate and 1% Triton X-100), supplemented with complete mini protease inhibitor tablets (Roche Applied Science, Laval, Quebec). Adrenal medullary homogenates were centrifuged for 5 min at 5,000 rpm. The resulting supernatants were collected and centrifuged for 30 min at 13,200 rpm. Protein concentrations were determined using the Dc Protein Assay Kit (Bio-Rad Laboratories, Hercules, CA). Equal amount of protein samples (10 µg for adrenal medulla and 30 µg for brain) were heated for 5 min at 95°C, separated on a 7% polyacrylamide gel and transferred onto a nitrocellulose membrane. To ensure equal loading of protein samples, blots were cut in two around 60 kDa. The lower parts of the blots were probed with a specific anti-β-actin antibody (Mono/Poly BD Biosciences, 1:5000). The upper parts of the blots were first probed for the Nav1.3 N-terminal (Sigma-Aldrich, Saint-Louis, clone 3F3, 1:500) and the Nav1.7 C-terminal (University of California (UC), Davis/National Institutes of Health NeuroMab Facility, clone N68/6, 1:500). Blots were incubated with a peroxydase-conjugated secondary antibodies and the signal was detected using the ECL-Plus Chemiluminescence kit (Amersham). Labelled blots were then exposed to Fujifilm Medical X-Ray Film to visualize antibody binding with a luminescent image analyser (LAS-3000, FUJIFILM). Intensities of Nav1.3 and Nav1.7 channel bands were normalized to those of β-actin and quantified using Image Gauge software.

Analysis - Data are given as mean ± SEM for n number of cells. Statistical significance was estimated with paired student t-tests in case two groups of measurements had to be compared and with a one way ANOVA followed by a Bonferroni post hoc analysis in case more than two groups had to be compared with one another. Data were found statistically significant when $p \leq 0.05$. Statistical analysis was performed with SPSS software (version 20.0, IBM). Data analysis was performed with pClamp and Origin (OriginLab Corporation, Northampton, MA, USA) software.

Results

Nav1.3 and Nav1.7 channel expression in mouse chromaffin cells

We first addressed by real-time RT-PCR the transcriptional expression profile of all known Nav channel isoforms. The data showed a differential expression of the six mRNAs (scn1a, scn2a, scn3a, scn4s, scn8a and scn9a) encoding Nav1.1, Nav1.2, Nav1.3, Nav1.4, Nav1.6 and Nav1.7 TTX-sensitive Nav channels respectively (Fig. 1a, left histogram). Among detectable isoforms (26<Ct<30), the rank order of the relative mRNAs abundance was scn3A > scn9a > scn2a > scn1a. Scn3a mRNA level was, ~7-fold higher as compared to scn9a (***p<0.001). Scn4a cDNA was amplified with a Ct of 35 and was thus considered not significantly expressed. Scn8a was undetectable. Messenger RNAs encoding all TTX-resistant Nav channels were detected at very low levels (Ct of 34 for scn5a and 35 for scn10a and scn11a) and therefore were considered absent from the mouse adrenal medulla tissue. We also examined the expression profile of the Nav channel auxiliary β subunits (Fig 1a, right histogram). Scn1b, 2b and 3b (β1-3 subunits were significantly expressed (26<Ct<28) while scn4b mRNA (β4 subunit) was considered absent (Ct of 35). Scn1b and scn2b subunits displayed comparable mRNA expression levels and scnb3 mRNA was found 1.7-fold more abundant than scnb1 subunit (**p<0.01). The expression of Nav1.3 and 1.7 were also investigated at the protein level by immunoblotting using specific antibodies. The western blots (macro-dissected adrenal medulla extracts) showed a strong immunoreactivity for a single band with an apparent molecular weight of ~230 kDa (Nav1.3) and ~220 kDa (Nav1.7) (Fig. 1b).

Altogether, qRT-PCR experiments and western blots indicate that voltage-gated Na^+ channels expressed in the mouse adrenal medullary tissue are likely formed by combination of β1-3 subunits with Nav α-subunits with a predominance of Nav1.3 and Nav1.7. These data are in agreement with previous electrophysiological studies showing that MCCs Nav channels are sensitive to TTX (Mahapatra et al, 2011; Vandael et al., 2012).

MCC Nav channels are TTX-sensitive and fully inactivating

Voltage-clamp recordings of Na^+ currents at -10 mV were carried out to validate TTX sensitivity as well as activation and inactivation properties of MCC Nav channels. TTX was perfused in gradually increasing concentrations and the degree of Na^+ current block with respect to control was fitted with a dose-response curve (Fig. 2a). Half maximal block was obtained at 6.7 ± 0.8 nM (n = 11) and saturation set at ~ 300 nM. This confirms the qRT-PCR data and proves that all α-subunits expressed in MCCs (in particular the two dominant ones: Nav1.3 and Nav1.7) are TTX-sensitive. Given this, we used subtraction of current traces measured in the presence of 300 nM TTX from control traces to obtain pure Na^+ currents. From this point on we will use Nav to refer to a mixture of Nav1.3 and Nav1.7 channels.

So far the activation properties of Na^+ channels have been described for bovine as well as rat CCs (Fenwick *et al.*, 1982; Lou *et al.*, 2003; Wada *et al.*, 2008). Nav channel activation properties have been studied also in MCCs (Mahapatra *et al.*, 2011) but many aspects remained unexplored. Of particular interest in excitable cells is the presence of persistent Na^+ currents as well as resurgent Na^+ currents (Raman & Bean, 1997; Bean, 2007). To test for the existence of persistent currents we opted for 1 s lasting depolarization steps, representing the average time a MCC spends between two consecutive spontaneous APs. It is known that besides the persistent nature of slow inactivating Na^+ currents, the activation kinetics of these currents are typically shifted to more negative V_m (French *et al.*, 1990; Magistretti *et al.*, 1999). These two features are thus ideally suited for a role in generating spontaneous membrane oscillations and can be exploited to help distinguish "persistent" from "transient" current components. All cells tested (n= 8) showed no direct signs of a persistent Na^+ current component (Fig. 2b). For potentials above -20 mV, time constants of channel inactivation (τ_{inact}) did not exceed 1 ms while for -40 and -30 mV we obtained τ_{inact} = 35.5 ± 11.9 ms and 12.7 ± 2.2 ms, respectively (Fig. 2e). Currents at steady-state did not show the typical bell-shaped current-voltage relationship (arrow in Fig. 2b) as we observed for the transient current component, which rose steeply with voltage and had half-maximal activation ($V_{½}$) at -21 mV. This suggests that we are mainly dealing with noise fluctuations near the baseline rather than steady-currents conducted by voltage-gated channels. Nevertheless, whole-cell Na^+ currents were too noisy at steady-state (1 s) to provide conclusive evidence in favour of the absence of persistent Na^+ currents. Since MCCs typically exhibit high input resistances (2-5 GΩ), small non-inactivating currents could lead to sizable membrane depolarizations and, thus, should be carefully evaluated. Based on our recordings we could estimate that these currents could not be larger than 1-2 pA.

Single Nav channel recordings in perforated micro-vesicles

To better test for the presence of a persistent Na^+ current in MCCs we studied the properties of single Na^+ channels in perforated micro-vesicles that were pulled out from a cell-attached configuration (Fig. 2c). This procedure leads to an excellent voltage control and allows one to validate the entity of the measured channels by selective blockers, maintaining the intracellular environment intact (Levitan & Kramer, 1990). Typically, micro-vesicles (n= 6 cells) were obtained containing 6 to 15 Nav channels. The total number of channels in a patch was estimated by the maximal number of superimposed channel openings at potentials of maximal activation (-10 mV) (Carbone & Lux, 1986). Levels were set based on unitary channel current amplitude that was revealed for each potential at steady-state and threshold based statistics were performed (see (Carabelli *et al.*, 2001; Carabelli *et al.*, 2002)). Most unitary events occurred soon after the onset of the depolarizing pulse and reopenings were observed for the whole duration of the recording. Unitary events became infrequent and dwell times were rather short lived (Fig. 2c,h). Based on the unitary current amplitudes at -40, -30 and -20 mV (distributed around a Gaussian function) we

could estimate a single channel conductance of 11 pS (Fig. 2d), in good agreement with single Nav channel recordings from bovine CCs (BCCs) (13 pS; (Fenwick *et al.*, 1982)) and chick dorsal root ganglion neurons (DRG) (11 pS; (Carbone & Lux, 1986)). Dwell time was measured at steady-state (200–1000 ms) since individual channel openings could be accurately followed in this time interval. Altogether the number of openings that were included in the analysis were 226, 243 and 111 for voltage steps to -40, -30 and -20 mV, respectively. Concerning the mean dwell time, single openings significantly increased in duration (***$p<0.001$; ANOVA, Bonferroni post hoc) at more depolarized potentials (-30 and -20 mV) as compared to -40 mV (Fig. 2f). This is in good agreement with reported values in BCCs (Fenwick *et al.*, 1982) and DRG neurons (Carbone & Lux, 1986) if our MCCs data were shifted by -10 to -15 mV to account for the different recording conditions (perforated vesicle vs. outside-out patch). As for the Nav channels of BCCs, the mean dwell time in MCCs was always below the inactivation time constant (τ_{inact}) of the ensemble current (mean dwell time 1.35 ms and mean τ_{inact} 2.0 ms at -20 mV) (Fig. 2e,f).

One disadvantage of using perforated micro-vesicles is the rare occurrence of obtaining single ion channel recordings. This issue limits the possibility to measure with accuracy the channel open probability (P_O). Since we were interested in persistent Na^+ currents (late openings), we measured P_O at steady state and divided for the total number of Nav channels estimated at -10 mV where all available Nav channels are expected to be open and the whole-cell current is maximal. P_O obtained in this way was extremely low ($P_O< 0.0025$ with $n = 6$ at -40 mV; Fig. 2g), suggesting that Na^+ channels are more transient than persistent. Even if in the worst case the openings at steady-state would represent only one single ion channel, open probabilities would not exceed 0.01, which would still be too low to be considered persistent. In stellate cells of the enthorinal cortex, persistent openings have been reported to result in P_O's of 0.1 to 0.9 (Magistretti *et al.*, 1999).

Finally the ensemble currents were constructed by summing up 10 consecutive traces as shown in Fig. 2c (bottom). Again we found a well-defined transient component with no signs of persistent inward currents at 1 s depolarization (shadowed traces in Fig 2c, bottom). The decay phase of the ensemble current was well fitted by a single exponential with τ_{inact} similar to the whole-cell recordings (Fig. 2e).

Nav channel inactivation in MCCs reduces the size of "window currents"

Availability of voltage-gated Nav channels depends critically on the holding potential (V_h) that the cell is clamped to. Given the transient nature of Nav channels and the low P_O, a critical factor that will determine the final steady-state current is how many channels will enter a V_h–dependent state of slow (ultraslow) inactivation. To find out we performed voltage-clamp experiments in which we simply stepwise depolarized the cell up to +60 mV ($\Delta V = 10$ mV) from a V_h varying from -100 mV to -30 mV (Fig. 3). As expected, the maximal current density significantly decreased by roughly 3 fold (**$p<0.01$) when the cell was kept at V_h = -40 mV as compared to -100 mV (Fig.

3b). Maximal current densities plotted versus V_h revealed a clear sigmoidal relationship (Fig. 4b) with half available Nav channels at -47.9 ± 1.9 mV. At V_h = -40 mV, availability of Nav channels reduces further to only 30%. This phenomenon will clearly reduce the Nav current amplitudes at critically low pacemaker potentials between -50 and -40 mV.

To quantify the current flowing at steady-state potentials we calculated the corresponding "window current" (Fig. 4a) by measuring activation and steady-state inactivation at diverse V_h (Fig. 3c). This latter was obtained by anticipating the test pulse at -10 mV (I_{max}) by a 100 ms lasting pre-pulse. Multiplying the activation curve by the inactivation curve gave the $P_o(V)$ (middle traces in Fig. 4a) that when multiplied by the whole-cell current (upper traces) led to the inward "window current" vs. voltage (bottom traces in Fig.4a). As expected, we found rather low P_O values at -40 mV (0.0035) compared to V_h -100 mV (0.009). The closer the values for half maximal activation and half-maximal inactivation, the bigger the overlap was between the relative activation and inactivation curve and the bigger the window current. We observed that the gap between half-maximal activation and inactivation became bigger as we fixed V_h to gradually more positive values. The discrepancy between both relative activation and inactivation doubled when we compared V_h -100 mV with V_h -40 mV (-21.4 ± 0.3 mV and -44.6 ± 0.7 mV for V_h -100 mV and -13.4 ± 0.3 mV and -59.7 ± 1.2 mV for V_h -40 mV) (Fig. 4c). It is thus not surprising that the window current we measured decreased from -15.6 pA at V_h -100 mV to -2.2 pA at V_h -40 mV. The fact that the window current is bell shaped and nearly zero around -20 mV, furthermore indicates that inactivation is complete towards more positive potentials. The inactivation curve of a "persistent current" would not fall to zero but rather would give robust currents at positive potentials (given the high relative channel availability at these voltages) (French et al., 1991). Altogether, channel availability, and activation/inactivation properties of Nav current in MCCs at physiologically relevant V_h (-50, -40 mV) do not favour sizeable steady-state currents that could drive spontaneous membrane oscillations.

Recovery from fast inactivation and onset of slow inactivation of Nav channels

Nav channels contributing to rhythmic firing should be able to recover enough Na^+ current between two consecutive APs to guarantee stable AP waveforms. We thus assayed the onset of recovery from fast inactivation by comparing the timing at V_h -90 mV with two physiological V_h representing the resting state (V_h = -50 mV) and a depolarized state that would occur during acute stress response (V_h= -40 mV; Fig. 5a). Recovery from fast inactivation in all three conditions occurred in a bi-exponential mode and striking differences were notable. Recovery was slow and remarkably incomplete (50%) after 1 s when V_h was set at -40 mV, while it was fast and fully complete (100%) at V_h -90 mV (Fig. 5a). The time constant of the dominant fast component (τ_{fast}, see figure legend) decreased from 23.7 ms (V_h -40 mV) to 4.9 ms (V_h -90 mV). A pulse of moderate duration (100 ms) starting from V_h -40 mV thus leads to a loss of about half of the available Nav channels that failed to recover.

It is known that beside fast inactivation, Nav channels can transit into a phase of slow inactivation from which the recovery can take several seconds (Cantrell & Catterall, 2001). Thus, the question is whether the incomplete recovery from inactivation at V_h -40 mV is due to a switch of channels into such a state of slow inactivation. To answer this question, we constructed a protocol where slow inactivation was induced by a strong depolarization to -10 mV, lasting up to 10 s. The Nav current before this pulse (I_1) was then compared with the current available after the conditioning step (I_2). Between the conditioning pulse and the second test pulse (I_2) the cell was kept at V_h for 1.2 s to allow for the recovery from fast inactivation (Fig. 5b). Data shown in Fig. 5b were fit with a 1st order exponential function with time constants that declined with increasing V_h. Nav current decay measured in this manner was 14 times faster for V_h -40 mV as compared to V_h -90 mV and 3 times faster as compared to V_h = -50 mV (τ = 7.8 ± 1.6 s for V_h -90; 1.64 ± 0.3 s for V_h -50 and 0.58 ± 0.63 s for V_h -40 mV). Thus, at physiologically relevant holding potentials a larger fraction of channels enter states from which recovery from inactivation is slower. This phenomenon is of relevance, when chromaffin cells are depolarized during stress responses. The incomplete recovery from fast inactivation and the fast onset of slow inactivation can thus produce a drastic reduction of available Nav channels at -40 and -50 mV.

Slow inactivation of Nav channels during slow ramp commands

So far we considered only square pulse protocols that do not represent the spontaneous membrane oscillations at rest. We thus tested the Nav current behaviour during slow gradual depolarizing pulses (ramp commands of 0.1 to 1 s) that mimic MCCs interspike intervals (ISIs). The ramps reached -20 mV, starting from two different V_h's (-40 mV and -50 mV). Currents evoked in this manner in both conditions were then compared (Fig. 5c). In line with the above findings, current amplitude was bigger (1.8 fold) when ramps of 100 ms duration were triggered from V_h= -50 mV as compared to -40 mV. With increasing ramp duration, currents decayed in an exponential manner both for V_h -50 mV (τ = 134 ± 15 s) and V_h -40 mV (τ = 160 ± 23 s). For ramps lasting 1 s, the remaining currents had mean amplitudes of -3.3 ± 1.2 pA for V_h = -50 mV and -2.5 ± 0.8 pA for V_h = -40 mV (Fig. 5c). Notice that, when the same protocol (V_h -50 mV) was performed, the L-type Ca^{2+} currents (LTCCs) were 8-fold bigger after 1 s lasting ramps (-25 ± 3.6 pA, Fig. 5c and inset). Together with the more negative activation kinetics, it is clear that LTCCs possess more suitable features to contribute to pacemaker depolarization than Nav channels do. Nav currents in fact activate at ~20 mV more depolarized potentials with respect to LTCCs (see Fig. 2A in Mahapatra et al., 2011) and inactivate fully during long ramp commands as shown in the bottom-right inset of Fig 5c.

It thus seems that the slow depolarization that anticipates the AP will carry a rather small (although not negligible) current and will probably inactivate the Na^+ current sustaining the spike upstroke. To test this hypothesis, we constructed a protocol where a fast ramp (20 ms) starting from spike threshold (-28 mV) and reaching +50 mV (I_2) was anticipated by a 1 s ramp (interspike

interval) that covers the pacemaker potential, i.e., from its most negative and most positive average values (-55 mV and -28 mV). These values represent the previously reported mean after-hyperpolarization peak (AHP = -53 mV) and mean spike threshold (-28 mV) (Vandael *et al.*, 2012). The resulting current was then compared to a ramp of 20 ms duration (I_1) elicited from -55 to +50 mV (Fig. 5d). Both ramp depolarizations were separated by intersweep intervals of 5 s to ensure complete recovery of Nav channels from fast inactivation. Nav currents were 14 times smaller during I_2 as compared to I_1 (-65 ± 17 pA vs. -889 ± 223 pA, n= 8; ***p<0.001, t-test). This suggests that during the pacemaker potential massive Nav channel inactivation occurs (Fig. 5d)..

Loss of Nav channels during depolarization profoundly modify the AP shape

Given the profound effects of V_h on Nav channel availability we assayed how this phenomenon affects MCCs firing and AP-waveform properties (Fig. 6). Experiments were performed in current-clamp mode without current injection. Cells in control conditions fired at 0.98 ± 0.08 Hz and V_{rest} was -46 ± 1.3 mV (n = 12). By injecting inward current to bring V_{rest} near -40 mV (-38.4 ± 1.0 mV), the firing frequency increased nearly 3-fold, (***p<0.001; t-test) accompanied by a significant widening of the AP half width (2.5 fold; ***p<0.001) and robust decrease of the peak overshoot (by ~25 mV; ***p<0.001) (Fig. 6a,b right). Averaged APs in control and after current injection were used to calculate *dV/dt,* which was then graphically visualized versus V_m in a phase plane plot (Fig. 6b, left). A massive reduction of dV/dt_{max} (~5 fold, ***p<0.001; t-test) is evident. This parameter represents the point where the AP rising phase is fastest during the up-stroke and is associated with Nav channel density (Bean, 2007). Altogether these changes point towards a strong decrease of Nav channel contribution to the AP at depolarized V_h. To confirm this we performed AP-clamp experiments, using trains of APs measured under control conditions and after depolarization (Fig. 6c). Clean Nav currents were obtained by final subtraction of control recordings from traces measured in the presence of 300 nM TTX (Fig. 6c). Comparison of Nav currents in control conditions (V_h= -50 mV) and at depolarized V_{rest} (V_h= -40 mV) showed marked reductions of Nav current amplitudes after each AP: ~60% at -40 mV and ~40% at -50 mV, respectively (*p<0.05) (Fig. 6c right)

Nav channel block by TTX leads to a switch from tonic to burst-like firings

As cell depolarization leads to a reduction in the contribution of Nav channels to the AP, we planned a series of experiments in which increasing fractions of Nav channels were pharmacologically blocked to test how Nav current availability may impact on firing patterns and spike parameters (Fig. 7). TTX was tested on spontaneously firing MCCs and applied at the same concentration used in voltage-clamp experiments (Fig. 2b). As previously reported (Vandael *et al.*, 2010; Mahapatra *et al.*, 2011), TTX did not impede the cell from generating spontaneous APs, not even at saturating concentrations (300 nM, Fig. 7a). As expected, we observed a dose-dependent reduction of the AP peak (IC_{50}= 9.0 ± 1.9 nM) and a dose-dependent increase of the half-width (IC_{50}= 18.7 ± 4.3 nM) (Fig. 7c,d). We also measured the coefficient of variance (CV =

SD/mean) for the ISI duration as an indication of the regularity of the firing pattern. The CV during control firing was 0.8 ± 0.01 and increased up to 1.1 ± 0.1 in the presence of 300 nM of TTX, indicating that in the absence of Nav channels the firing pattern is clearly more irregular.

A closer look at the firing patterns after Nav channel block shows the tendency of MCCs to fire its APs preferentially in bursts, especially at saturating doses of TTX (Fig. 7b). The switch from tonic to burst-like firing is particularly evident in the distributions of the ISI duration (Fig. 7b, center). In control conditions the distribution is nearly random (low CV) while at increasing TTX concentrations two separate Gaussian distributions with distinct peaks become evident. The first peak (brief durations) represents ISIs between two consecutive spikes in a burst (*intra-burst interval*) while the second peak at longer times represents the ISI between bursts (*inter-burst interval*). The centres of the Gaussian for the intraburst interval varied from 77.1 to 57.8 ms by increasing TTX from 30 to 300 nM, while the Gaussian of the interburst intervals centred at 1.1 to 1.3 s.

When we subsequently plotted each ISI against its preceding ISI duration we could distinguish a clear difference between control and Nav block-induced firing patterns (Fig. 7b, bottom). In these so called *joint-interspike-interval* plots, irregular "tonic" firing patterns give rise to a cloudy distribution of events while "burst" firing gives rise to an "L-shaped" distribution. The L-shaped joint interspike interval can be ascribed to the prevalence of altering long with peculiarly brief ISIs during a burst. Together with a change in the ISI distribution there was also a dose dependent percentage increase (IC_{50} of 38.9 ± 9.8 nM) of spikes fired in bursts with increasing doses of TTX (Fig. 7e). The parameter that was most sensitive to TTX was the AP amplitude (IC_{50}= 9.0 nM; Fig. 7c), followed by the half-width (IC_{50}= 18.7 nM; Fig. 7d) and the percentage of spikes fired in bursts (Fig. 7e). Out of 16 cells, the overall firing frequency was increased after Nav channel block as compared to control while in 3 cells we observed a decrease.

Altogether we did not observe a significant difference (*p>0.05) for the firing frequency when control conditions (0.9 ± 0.1 Hz) were compared with firing that persisted after Nav channel block (1.2 ± 0.2 Hz). During burst firing however, brief periods of high frequency firing (14.8 ± 1.2 Hz; n= 16) were altered by relatively long gaps of no activity. In addition, spikes fired in bursts emerge from depolarization plateaus (-38.7 ± 1.3 mV up to -33.1 ± 1.2 mV) that last for the whole burst duration. It is thus possible that Ca^{2+} influx is particularly high during such firing patterns and an increased degree of catecholamine secretion takes place.

Reduced Nav availability inverts the net current during the AHP from outward to inward

Fig. 7 shows clearly that a reduction of Na^+ current amplitude upon cell depolarization leads to broad and low amplitude spikes that oscillate in a voltage range where the driving force on Ca^{2+} ions is high. Less Nav channel availability leads to less K_V and BK channel activation since cells do not reach positive membrane potentials during the AP peak and this in turn will lead to slower return to baseline potentials. Of particular interest is the effect of this phenomenon on the

currents flowing during the AHP. A possible switch from a net outward to a net inward current could explain the development of a sufficiently low AHP that drives the burst of APs when Nav channel availability is drastically reduced.

To better understand this issue we performed AP-clamp experiments in which we aimed to unravel the balance between outward K^+ and inward Ca^{2+} currents during APs measured in 3 conditions: 1) control firing patterns, 2) depolarized V_h potentials, and 3) burst firing in 300 nM TTX (Fig. 8). Ca^{2+}-activated K^+ currents (IK_{Ca}) were isolated by subtraction of the whole-cell Ca^{2+} current (measured in 135 mM TEA, 2 mM Ca^{2+} and 300 nM TTX) and the K_V current (IK_V) (Tyrode standard with 200 µM of Cd^{2+} and TTX) from the total current measured in Tyrode standard with 300 nM TTX. Compared to control spikes, we observed a 4-fold reduction of IK_V flowing during spikes that started from a depolarized membrane potential (**p<0.01, n= 9) and a 25-fold reduction during the burst doublets in the presence of 300 nM TTX (***p<0.001, n= 9). Note that during the APs burst, IK_V is nearly absent (Fig. 8c, red trace) and IK_{Ca} is drastically reduced (blue trace; *p<0.05, n= 9). The net current during the spikes remained outward, justifying the effective repolarizing phase in all three conditions. However, marked changes were observed during the AHP. While the net current during the AHP of control spikes was outward, the current during the intraburst interval was net inward and carried by Ca^{2+} (inset in Fig. 8b). It thus results that incoming Ca^{2+}, together with a lack of sufficient outward K^+ current is the trigger of burst firing when Nav channels are blocked. Broadening of APs during cell depolarization and bursts of APs in the presence of TTX caused a 2- to 10-fold prolongation of Ca^{2+} currents (bottom insets in Fig. 8a-c) that, despite the lower amplitudes, could carry 2- and 3.5-fold more Ca^{2+} charges inside the cell, respectively (inset in Fig. 8c).

A minority of MCCs exhibits spontaneous burst firing

Spontaneous burst firing (zero current injected) was also observed in a minority of cells (14%, 39 out of 278) that were measured in current clamp (Fig. 9a). A train of high frequency spikes emerged on a “slow-wave” depolarization plateau with somewhat different shape and duration but comparable frequency of those induced by TTX. Burst durations were 2.6 fold longer (0.37 ± 0.08 s vs. 0.14 ± 0.03 s with TTX; ***p<0.001 with unpaired t-test) but occurred at nearly the same frequency (0,56 ± 0.09 Hz vs. .0,48 ± 0.15 Hz). Due to the Nav channel availability, the first spike overshoot was always larger as compared to the subsequent APs. Spikes showed a gradual reduction in peak amplitude (from +16.3 to -10.11 mV, ***p<0.001: paired t-test), a sequential increase in half width duration (from 2.9 to 6.8 ms, ***p<0.001) and reduction in AHP amplitude (from -41 to -34.4 mV, ***p<0.001) (Fig. 9b). The intraburst interspike interval duration and thus also the intraburst instantaneous firing frequency furthermore increased strongly towards the end of the burst (from 170.3 to 65.3 ms and from 8.9 to 21.2 Hz respectively, ***p 0.001). Again we hypothesized that Nav channel inactivation leads to a reduction in the AP peak that leads to less K_V activation and thus spike broadening. The low amplitude spikes could furthermore explain the

gradual reduction in the AHP that helps shape the burst envelope. In order to quantify this we performed AP-clamp recordings using bursts as voltage clamp commands (Fig. 9c-e). When considering Na^+-currents we found that the amplitudes significantly (***p<0.001, n= 6) decreased by 15-fold comparing the currents elicited during the first- and last spike of the burst (Fig. 9f). This is not surprising given that the narrow interspike intervals do not allow enough time for recovery from inactivation. In addition, gradually decreasing AHP and spike broadening lead to an increased depolarization and, thus, more complete Nav inactivation. A decrease of outward currents also occurred. K_V currents reduced by 4.4 fold (***p<0.001, n= 18) while BK current amplitudes decrease by 5.6 fold (***p<0.001, n= 7) comparing currents during the first and last spike (Fig. 9f). Ca^{2+}-current amplitudes reduced by 3 fold (***p<0.001, n= 17) but when we measured the area under the curve we found a 1.7 fold increase (***p<0.001) in Ca^{2+}-charge (Fig. 9f). In line with the idea of Ca^{2+} building up with each and every spike we found a sequential and significant increase in SK current amplitudes (***p<0.001, n= 7) (Fig. 9f). It is worth noticing that the decrease of Nav, Kv, BK and Cav current amplitude during consecutive APs is not due solely to inactivation but also to the decreasing amplitude of the APs in the command waveform.

Block of Nav channels boosts MCCs exocytosis

Bursts of APs originating from plateau potentials of -35 mV, lasting for hundreds of milliseconds thus go hand in hand with an increase of inflowing Ca^{2+}-charge (Fig. 8c and Fig. 9e,f). One can hypothesize that the block of TTX-sensitive Nav channels paradoxically leads to an increased Ca^{2+}-dependent secretion of catecholamines in MCCs due to both the sustained depolarization (slow-wave) and the increased AP frequency during bursts. To test this, we combined current-clamp recordings with carbon fibre amperometry to reveal fast quantal release of catecholamines during MCCs firing patterns (for 40 s) at rest and after Nav block (Fig. 10) (Carabelli *et al.*, 2007b). Cells were hyperpolarized to -70 mV in order to cease spontaneous activity and to prevent Ca^{2+} accumulation at the onset of the recording. Subsequently inhibition was relieved and spontaneous activity was measured for 40 s. As expected, in the presence of TTX all cells switched from a tonic (Fig. 10a) into a burst-firing mode (Fig. 10b). Amperometric signals associated with vesicle fusion and catecholamine release were detected in both cases but at significantly different frequency. Block of Nav channels by TTX caused a nearly 2.5-fold increase of the rate of vesicle release with respect to control (*p<0.05; n= 14) (Fig. 10d bottom) with no significant changes to the waveform of amperometric spikes (Fig. 10d top). The parameters associated with the peak amplitude (I_{max}), time to peak (t_p), half-width ($t_{1/2}$), rise time (m), total quantity of charge released (Q) and cubic root of Q ($Q^{1/3}$) (as an estimate of vesicle size) remained unchanged (*p>0.05, t-test), regardless of the Nav channel block and the switch of cell firing mode (Fig. 10d). We also determined the time course of cumulative secretion (Fig. 10c) and calculated the mean quantity of cumulative charges recorded during a 40 s recording and found a

3.7-fold increase of the cumulative charge (Fig. 10d). As shown previously (Marcantoni *et al.*, 2009), this can be explained by the increase of the amperometric spike frequency (2.5-fold) which may sum to a small net charge increase of the single secretory events not sufficiently large to be detected (Fig. 10d). Given that the quantity of Ca^{2+} charges is linearly related to the amount of released vesicles in CCs (Carabelli *et al.*, 2003; Carabelli *et al.*, 2007a), the 2.5-fold increased frequency of amperometric spikes and the 3.7-fold increase of cumulative released charges in the presence of TTX are in very good agreement with the 3.5-fold increase of Ca^{2+}-entry during bursts of APs (Fig. 8c).

On average, five APs are required to elicit an exocytotic event in RCCs in control conditions (1.1 Hz APs vs 0.2 Hz amperometric spikes) (Zhou & Misler, 1995). We found that the same occurs in MCCs. Specifically, we found no strict correlation between APs and amperometric events in both control conditions or during burst firing induced by TTX. During burst firing, periods of elevated vesicle release sometimes occurred during the gaps that separated the bursts rather than during the bursts themselves. It is thus evident that Ca^{2+} has to diffuse in the cell in order to trigger most of the exocytotic events. It is important to underline that our data do not allow distinguishing whether the increased secretion in the presence of TTX is mainly due to Ca^{2+}-entry during the slow-wave depolarization or to the increased frequency of APs riding on top of the slow wave. Both phenomena occur simultaneously and cause increased Ca^{2+}-influx, whose separation requires specific protocols.

Discussion

We have provided evidence that Nav channels are not mandatory to generate spontaneous APs in MCCs. APs persist in the presence of saturating doses of TTX and contribution of persistent or resurgent Nav channels to pacemaking is null. We have shown here that, similar to TTX, small depolarizations from rest drastically lower Nav channel availability mostly due to incomplete recovery from fast inactivation and fast onset of closed-state inactivation. Like TTX, this causes drastic changes in AP-shape and firing patterns that increases Ca^{2+}-entry and catecholamine release. Since Nav channel down-regulation is implicated in the control of input-output relationships in several neurons, a key implication of our findings is that gradual loss of Nav channels may drastically change electrical excitability of neuroendocrine cells (Cantrell & Catterall, 2001).

Expression profile of the fast-inactivating TTX-sensitive Nav channels of MCCs

Previously, scn9a (Nav1.7) has been thought to be the principal Nav α-subunit gene expressed in the adrenal medulla (Klugbauer *et al.*, 1995; Morinville *et al.*, 2007; Wada *et al.*, 2008; Yanagita *et al.*, 2011). Our expression data confirm the presence of scn9A in MCCs but, surprisingly, uncover a 7.3-fold higher expression level of scn3A transcripts (Nav1.3). Both isoforms are confirmed at

the protein level and it cannot be excluded that Nav1.1 and Nav1.2 are expressed despite their low-degree of transcripts. The absence of the mRNA of TTX-resistant Nav isoforms such as scn5A (Nav1.5), scn10A (Nav1.8) and scn11A (Nav1.9) supports our data that saturating doses of TTX block all Nav currents (IC_{50} ~7nM). Half-maximal Nav block by TTX is comparable with that reported for Nav1.7 and Nav1.3 (IC_{50} ~4 nM) (Sangameswaran *et al.*, 1997; Catterall *et al.*, 2005), which are the main Nav channels expressed by MCCs. Our Nav activation data ($V_{1/2}$= -21 mV) on MCCs fit with those reported for BCCs (Fenwick *et al.*, 1982) and RCCs (Lou *et al.*, 2003; Wada *et al.*, 2008) and are also in good agreement with the reported values for Nav1.3 and Nav1.7 α-subunits expressed in HEK cells ($V_{1/2}$= -26 mV; (Catterall *et al.*, 2005)). Based on their $V_{1/2}$ of activation and inactivation and their kinetics of recovery from fast inactivation and onset of slow closed-state inactivation, Nav1.3 and Nav1.7 are nearly indistinguishable except for the slower recovery of inactivation of Nav1.7 with respect to Nav1.3 (26 vs. 11 ms at V_h= -100 mV and 113 vs. 60 ms at V_h= -80 mV) (see table 1 in (Cummins *et al.*, 2001)). These latter values, however, are too small to be associated to the slow component of the recovery of inactivation of Nav channels in MCCs (156 to 501 ms; Fig. 5a), whose cause remains to be clarified. Compared to Nav1.2 both channels display a marked slow entry rate in the closed-state inactivation, which makes both of them suitable for sustaining robust responses to slowly depolarizing inputs. This and the absence of reported values on the single channel conductance of Nav1.3 (Catterall *et al.*, 2005) makes it nearly impossible to associate the functional Nav channel properties of MCCs to either Nav1.3 or Nav1.7. This issue would certainly benefit from analysis of the Nav currents of MCCs in Nav1.3 (Nassar *et al.*, 2006) and Nav1.7 null mice (Nassar *et al.*, 2004).

Our whole-cell data and single-channel recordings confirm that MCC Nav currents are not persistent. Sustained Nav currents are typically associated with the Nav1.6 isoform (scn8a) (Raman & Bean, 1997), which activates at potentials as negative as -70 mV (Taddese & Bean, 2002) and sustains tonic-firing at elevated frequencies (20-100Hz) in several neurons (Smith *et al.*, 1998; Rush *et al.*, 2005; Enomoto *et al.*, 2007; Mercer *et al.*, 2007). MCCs do not fire at elevated frequencies and lack scn8a. In addition, the auxiliary subunit scn4b ($Na_V\beta4$) is linked to resurgent Na^+ currents (Bant & Raman, 2010). Neither scn4b nor resurgent Na^+ currents were revealed in MCCs.

Nav1.3/Nav1.7 channel contribution to MCC auto-rythmicity

Early reports have shown that Nav channels are critically involved in driving AP firing in gerbil and human CCs (Biales *et al.*, 1976). Recording conditions in these studies were nevertheless strikingly different from ours (perforated-patch in 2 mM Ca^{2+} vs. sharp-electrode impalement in 10 mM Ca^{2+}) and cells were more depolarized (-40 to -10 mV) than MCCs (-50 to -45 mV). A similar approach on RCCs resulted in a V_{rest} ~-49 mV and TTX strongly interfered with AP generation (Brandt *et al.*, 1976). The present general belief is that Nav1.7 represents the main Nav channel isoform in bovine and rat adrenal glands (Klugbauer *et al.*, 1995; Morinville *et al.*, 2007; Wada *et*

al., 2008). Nav1.7 possesses slow closed-state inactivation during very negative ramp depolarizations, a feature that favours its contribution to auto-rythmicity (Lou *et al.*, 2003). We report here that Nav1.3 is highly expressed in MCCs and like Nav1.7 undergoes strong inactivation during prolonged depolarizations (Cummins *et al.*, 2001). MCC Nav channels can inactivate considerably during ramp-depolarizations mimicking the velocity of the interspike depolarization from physiological V_hs (Fig. 5c,d).

An important factor that influences Nav channel availability in MCCs is the relatively depolarized V_h. Between -50 and -40 mV, Nav availability ranges from 50% to 30%. We report moreover drastic changes in recovery from inactivation at physiologically relevant V_h. At -40 mV, recovery of inactivation remains fast (τ= 24 ms) but is strikingly incomplete due to the transition into a slow-inactivation state. The AP amplitude and the velocity of the spike upstroke strongly depend on the amount of available Nav channels. The 'vulnerability' of MCC Nav channels to inactivation is indeed reflected in profound changes of AP shape when cells are depolarized to -40 mV. At such depolarized potentials the Nav window-current is peculiarly small due to the shift of the inactivation curve to more negative potentials. Opposing shifts of both activation and inactivation curves (as occurs in MCCs when changing V_h from -100 to -40 mV) are expected to slow-down the frequency of tonic firing, indicating their effective contribution to pacemaking. This is true for dopaminergic neurons of the *substantia nigra* where Nav channels contribute to pacemaking (Tucker *et al.*, 2012) but is opposite to what we find in MCCs in which firing is accelerated. The fact that saturating doses of TTX do not interfere with spontaneous AP generation is conclusive evidence that Nav channels are not required for MCC pacemaking. Activation threshold for Nav channels occurs at more positive voltages than the MCC interspike interval (-46 mV), suggesting that a channel like the L-type Cav1.3 is required to bridge the gap (Marcantoni *et al.*, 2010; Vandael *et al.*, 2012).

Physiological relevance of Nav currents in MCCs: switch from tonic to burst-firing

Fast-firing cells typically exhibit very narrow APs with small overshoots and fast AP-repolarization (Bean, 2007). In this way, Nav inactivation is kept incomplete and contributes to fast firing phenotypes (Carter & Bean, 2010). Here, we clearly show that upon sustained depolarization, the AP peak of MCCs gradually drops and broadens, reducing the velocity of spike depolarization and repolarization. Such broad and low amplitude spikes are correlated with strongly reduced Na^+ current amplitudes (by 50% compared to V_{rest}). Nav1.3/Nav1.7 block by TTX leads to similar dose-dependent changes of AP waveform. In fact, TTX blocks with nearly the same IC_{50} both AP peak and Nav currents (9 vs.7 nM). This is different from several neurons that at V_{rest} ~-70 mV possess high-densities of Nav channels and the AP-shape is less sensitive to TTX (Madeja, 2000). MCCs have a lower surplus of Nav1.3/Nav1.7 channels whose availability is thus extremely sensitive to slight changes in membrane potential or channel down-regulation.

An interesting finding of our work is that saturating doses of TTX do not lead to a cessation of

firing but rather triggers a switch from single irregular APs into burst firing. Crucial to burst firing is the inward/outward current balance in between spikes (Swensen & Bean, 2003) and we have shown here that blocking Nav channels inverts the net outward K^+ current during the AHP to a net inward Ca^{2+} current. Similar changes on AP shape have been observed during TTX application or K^+ channel block by TEA on spontaneously active MCCs in the intact adrenal gland (Nassar-Gentina *et al.*, 1988). Spontaneous burst firing occurs also in a minority of MCCs (Fig. 9) but it occurs also in a small fraction of MCCs of adrenal slices (Martinez-Espinosa *et al.*, 2014). These authors also show that burst firing occurs in the majority of MCCs in which the β2-subunit of fast-inactivating BK channels is deleted. Thus, burst-firing appears as an intrinsic firing mode in a subpopulation of MCCs and may be easily uncovered during altered cell conditions. The final output is an increased Ca^{2+}-entry that boosts cell activity and secretion.

Firing modes regulate catecholamine release in chromaffin cells

We found an excellent correlation between the 3.5-fold enhanced Ca^{2+}-entry during the TTX-induced burst firing and the 3.7-fold increased total charges of released catecholamines. This is expected given the linear-dependence of Ca^{2+}-entry and catecholamine release in MCCs (Marcantoni *et al.*, 2009) and RCCs (Carabelli *et al.*, 2003), which derives from the weak coupling of Ca^{2+}-channels to the release sites (Marcantoni *et al.*, 2008). Whether the major source of Ca^{2+}-influx required for secretion in MCCs is due to the slow-wave depolarization or to the increased AP frequency during bursts remains to be solved. Nevertheless, it is interesting to recall that secretion in RCCs is more sensitive to stimulations in form of repeated bursts rather than single AP-trains of increasing frequency (Duan *et al.*, 2003). In midbrain dopaminergic neurons bursting stimulations are twice as potent in triggering secretion as regular spaced ones, having the same average frequency (Gonon, 1988).

The action of TTX reported here is unique. The toxin does not block the Ca^{2+}-dependent release of catecholamines, but rather increases it. In PC12 cells catecholamine release is fully Ca^{2+}-dependent and TTX preserves rather than blocking it (Ritchie, 1979). In intact perfused rat adrenal glands, 300 nM TTX leads to a reduction of ~43% of catecholamine secretion after transmural stimulation (Wakade, 1981). This apparent conflicting result may correlate with our data by assuming that the used TTX concentration was not sufficient to guarantee an efficient block of Nav channels in the whole-gland or that TTX could have partially blocked the Nav channels of presynaptic splanchnic nerve endings. In our hands RCCs pacemaking is more sensitive to Nav channel block (Martin *et al.*, 2001). A species-dependent origin of these divergent results is likely.

Our study indicates that loss or down-regulation of Nav channels is a critical process that leads to alteration of the AP waveform. In extreme situations, this phenomenon might lead to a switch in slow waves of burst firing that boost Ca^{2+}-entry inside the cell. In physiological conditions, this may occur under plasma hyperkalemia, acidosis or increased histamine levels at which CCs

respond with sustained depolarizations, burst firing (Wallace *et al.*, 2002; Inoue *et al.*, 2008; Mahapatra *et al.*, 2011) and enhanced circulating catecholamines (Clausen, 1983). Of particular interest in CC biology is the potential role of muscarinic receptors, whose activation causes prolonged membrane depolarizations, increased cell firing and sustained catecholamines release (Nassar-Gentina *et al.*, 1988; Olivos & Artalejo, 2007). The action is mediated by the M1 muscarinic receptor and proceeds through the inhibition of TASK1-like channels (Inoue *et al.*, 2008). As muscarine activates the PKC pathway in RCCs (Akaike *et al.*, 1993), it is likely that Nav channels may undergo the well known PKC-dependent down-regulation mediated by muscarinic receptors (Carr *et al.*, 2003). This, together with the 30% reduced Nav channels availability at depolarized V_h, would critically increase the probability of MCCs to switch into burst-firing patterns, boosting catecholamine release during ACh-driven acute stress responses.

References

Akaike A, Sasa M, Tamura Y, Ujihara H & Takaori S. (1993). Effects of protein kinase C on the muscarinic excitation of rat adrenal chromaffin cells. *Japanese journal of pharmacology* **61,** 145-148.

Bant JS & Raman IM. (2010). Control of transient, resurgent, and persistent current by open-channel block by Na channel beta4 in cultured cerebellar granule neurons. *Proc Natl Acad Sci U S A* **107,** 12357-12362.

Bean BP. (2007). The action potential in mammalian central neurons. *Nature reviews Neuroscience* **8,** 451-465.

Berkefeld H & Fakler B. (2013). Ligand-gating by Ca2+ is rate limiting for physiological operation of BK(Ca) channels. *The Journal of neuroscience : the official journal of the Society for Neuroscience* **33,** 7358-7367.

Biales B, Dichter M & Tischler A. (1976). Electrical excitability of cultured adrenal chromaffin cells. *The Journal of physiology* **262,** 743-753.

Brandt BL, Hagiwara S, Kidokoro Y & Miyazaki S. (1976). Action potentials in the rat chromaffin cell and effects of acetylcholine. *The Journal of physiology* **263,** 417-439.

Cantrell AR & Catterall WA. (2001). Neuromodulation of Na+ channels: an unexpected form of cellular plasticity. *Nature reviews Neuroscience* **2,** 397-407.

Carabelli V, D'Ascenzo M, Carbone E & Grassi C. (2002). Nitric oxide inhibits neuroendocrine Ca(v)1 L-channel gating via cGMP-dependent protein kinase in cell-attached patches of bovine chromaffin cells. *Journal of Physiology-London* **541,** 351-366.

Carabelli V, Giancippoli A, Baldelli P, Carbone E & Artalejo AR. (2003). Distinct potentiation of L-type currents and secretion by cAMP in rat chromaffin cells. *Biophysical journal* **85,** 1326-1337.

Carabelli V, Hernandez-Guijo JM, Baldelli P & Carbone E. (2001). Direct autocrine inhibition and cAMP-dependent potentiation of single L-type Ca2+ channels in bovine chromaffin cells. *Journal of Physiology-London* **532,** 73-90.

Carabelli V, Marcantoni A, Comunanza V & Carbone E. (2007a). Fast exocytosis mediated by T- and L-type channels in chromaffin cells: distinct voltage-dependence but similar Ca2+-dependence. *European Biophysics Journal with Biophysics Letters* **36,** 753-762.

Carabelli V, Marcantoni A, Comunanza V, De Luca A, Diaz J, Borges R & Carbone E. (2007b). Chronic hypoxia up-regulates alpha(1H) T-type channels and low-threshold catecholamine secretion in rat chromaffin cells. *Journal of Physiology-London* **584,** 149-165.

Carbone E & Lux HD. (1986). Sodium-Channels in Cultured Chick Dorsal-Root Ganglion Neurons. *European Biophysics Journal with Biophysics Letters* **13,** 259-271.

Carbone E & Lux HD. (1987). Single low-voltage-activated calcium channels in chick and rat sensory neurons. *Journal of Physiology-London* **386,** 571-601.

Carr DB, Day M, Cantrell AR, Held J, Scheuer T, Catterall WA & Surmeier DJ. (2003). Transmitter modulation of slow, activity-dependent alterations in sodium channel availability endows neurons with a novel form of cellular plasticity. *Neuron* **39,** 793-806.

Carter BC & Bean BP. (2010). Sodium entry during action potentials of mammalian neurons: incomplete inactivation and reduced metabolic efficiency in fast-spiking neurons. *Neuron* **64,** 898-909.

Catterall WA, Goldin AL & Waxman SG. (2005). International Union of Pharmacology. XLVII. Nomenclature and structure-function relationships of voltage-gated sodium channels. *Pharmacological reviews* **57,** 397-409.

Cesetti T, Hernandez-Guijo JM, Baldelli P, Carabelli V & Carbone E. (2003). Opposite action of beta 1- and beta 2-adrenergic receptors on Ca(V)1 L-channel current in rat adrenal chromaffin cells. *Journal of Neuroscience* **23,** 73-83.

Clausen T. (1983). Adrenergic control of Na+-K+-homoeostasis. *Acta medica Scandinavica Supplementum* **672,** 111-115.

Colborn JM, Byrd BD, Koita OA & Krogstad DJ. (2008). Estimation of copy number using SYBR Green: confounding by AT-rich DNA and by variation in amplicon length. *The American journal of tropical medicine and hygiene* **79,** 887-892.

Cummins TR, Aglieco F, Renganathan M, Herzog RI, Dib-Hajj SD & Waxman SG. (2001). Nav1.3 sodium channels: rapid repriming and slow closed-state inactivation display quantitative differences after expression in a mammalian cell line and in spinal sensory neurons. *The Journal of neuroscience : the official journal of the Society for Neuroscience* **21,** 5952-5961.

de Diego AM, Gandia L & Garcia AG. (2008). A physiological view of the central and peripheral mechanisms that regulate the release of catecholamines at the adrenal medulla. *Acta Physiol (Oxf)* **192,** 287-301.

Desarmenien MG, Jourdan C, Toutain B, Vessieres E, Hormuzdi SG & Guerineau NC. (2013). Gap junction signalling is a stress-regulated component of adrenal neuroendocrine stimulus-secretion coupling in vivo. *Nat Commun* **4,** 2938.

Duan K, Yu X, Zhang C & Zhou Z. (2003). Control of secretion by temporal patterns of action potentials in adrenal chromaffin cells. *The Journal of neuroscience : the official journal of the Society for Neuroscience* **23,** 11235-11243.

Engel D & Jonas P. (2005). Presynaptic action potential amplification by voltage-gated Na+ channels in hippocampal mossy fiber boutons. *Neuron* **45,** 405-417.

Enomoto A, Han JM, Hsiao CF & Chandler SH. (2007). Sodium currents in mesencephalic trigeminal neurons from Nav1.6 null mice. *Journal of neurophysiology* **98,** 710-719.

Fenwick EM, Marty A & Neher E. (1982). Sodium and calcium channels in bovine chromaffin cells. *The Journal of physiology* **331,** 599-635.

French CR, Sah P, Buckett KJ & Gage PW. (1990). A voltage-dependent persistent sodium current in mammalian hippocampal neurons. *The Journal of general physiology* **95,** 1139-1157.

Garcia AG, Garcia-De-Diego AM, Gandia L, Borges R & Garcia-Sancho J. (2006). Calcium signaling and exocytosis in adrenal chromaffin cells. *Physiol Rev* **86,** 1093-1131.

Gonon FG. (1988). Nonlinear relationship between impulse flow and dopamine released by rat midbrain dopaminergic neurons as studied by in vivo electrochemistry. *Neuroscience* **24,** 19-28.

Guerineau NC, Desarmenien MG, Carabelli V & Carbone E. (2012). Functional chromaffin cell plasticity in response to stress: focus on nicotinic, gap junction, and voltage-gated Ca2+ channels. *J Mol Neurosci* **48,** 368-386.

Inoue M, Harada K, Matsuoka H, Sata T & Warashina A. (2008). Inhibition of TASK1-like channels by muscarinic receptor stimulation in rat adrenal medullary cells. *Journal of neurochemistry* **106,** 1804-1814.

Kidokoro Y & Ritchie AK. (1980). Chromaffin cell action potentials and their possible role in adrenaline secretion from rat adrenal medulla. *The Journal of physiology* **307,** 199-216.

Klugbauer N, Lacinova L, Flockerzi V & Hofmann F. (1995). Structure and functional expression of a new member of the tetrodotoxin-sensitive voltage-activated sodium channel family from human neuroendocrine cells. *The EMBO journal* **14,** 1084-1090.

Levitan ES & Kramer RH. (1990). Neuropeptide modulation of single calcium and potassium channels detected with a new patch clamp configuration. *Nature* **348,** 545-547.

Li L, Bischofberger J & Jonas P. (2007). Differential gating and recruitment of P/Q-, N-, and R-type Ca2+ channels in hippocampal mossy fiber boutons. *J Neurosci* **27,** 13420-13429.

Lou XL, Yu X, Chen XK, Duan KL, He LM, Qu AL, Xu T & Zhou Z. (2003). Na+ channel inactivation: a comparative study between pancreatic islet beta-cells and adrenal chromaffin cells in rat. *The Journal of physiology* **548,** 191-202.

Madeja M. (2000). Do neurons have a reserve of sodium channels for the generation of action potentials? A study on acutely isolated CA1 neurons from the guinea-pig hippocampus. *The European journal of neuroscience* **12,** 1-7.

Magistretti J, Ragsdale DS & Alonso A. (1999). High conductance sustained single-channel activity responsible for the low-threshold persistent Na(+) current in entorhinal cortex neurons. *The Journal of neuroscience : the official journal of the Society for Neuroscience* **19,** 7334-7341.

Mahapatra S, Marcantoni A, Vandael DHF, Striessnig J & Carbone E. (2011). Are Ca(v)1.3 pacemaker channels in chromaffin cells? Possible bias from resting cell conditions and DHP blockers usage. *Channels* **5,** 219-224.

Marcantoni A, Baldelli P, Hernandez-Guijo JM, Comunanza V, Carabelli V & Carbone E. (2007). L-type calcium channels in adrenal chromaffin cells: role in pace-making and secretion. *Cell Calcium* **42,** 397-408.

Marcantoni A, Carabelli V, Comunanza V, Hoddah H & Carbone E. (2008). Calcium channels in chromaffin cells: focus on L and T types. *Acta Physiologica* **192,** 233-246.

Marcantoni A, Carabelli V, Vandael DH, Comunanza V & Carbone E. (2009). PDE type-4 inhibition increases L-type Ca2+ currents, action potential firing, and quantal size of exocytosis in mouse chromaffin cells. *Pflugers Archiv-European Journal of Physiology* **457,** 1093-1110.

Marcantoni A, Vandael DHF, Mahapatra S, Carabelli V, Sinnegger-Brauns MJ, Striessnig J & Carbone E. (2010). Loss of Cav1.3 Channels Reveals the Critical Role of L-Type and BK Channel Coupling in Pacemaking Mouse Adrenal Chromaffin Cells. *Journal of Neuroscience* **30,** 491-504.

Martin AO, Mathieu MN, Chevillard C & Guerineau NC. (2001). Gap junctions mediate electrical signaling and ensuing cytosolic Ca2+ increases between chromaffin cells in adrenal slices: A role in catecholamine release. *The Journal of neuroscience : the official journal of the Society for Neuroscience* **21,** 5397-5405.

Martinez-Espinosa PL, Yang C, Gonzalez-Perez V, Xia XM & Lingle CJ. (2014). Knockout of the BK beta2 subunit abolishes inactivation of BK currents in mouse adrenal chromaffin cells and results in slow-wave burst activity. *The Journal of general physiology* **144,** 275-295.

Mercer JN, Chan CS, Tkatch T, Held J & Surmeier DJ. (2007). Nav1.6 sodium channels are critical to pacemaking and fast spiking in globus pallidus neurons. *The Journal of neuroscience : the official journal of the Society for Neuroscience* **27,** 13552-13566.

Morinville A, Fundin B, Meury L, Jureus A, Sandberg K, Krupp J, Ahmad S & O'Donnell D. (2007). Distribution of the voltage-gated sodium channel Na(v)1.7 in the rat: expression in the autonomic and endocrine systems. *The Journal of comparative neurology* **504,** 680-689.

Nassar-Gentina V, Pollard HB & Rojas E. (1988). Electrical activity in chromaffin cells of intact mouse adrenal gland. *The American journal of physiology* **254,** C675-683.

Nassar MA, Baker MD, Levato A, Ingram R, Mallucci G, McMahon SB & Wood JN. (2006). Nerve injury induces robust allodynia and ectopic discharges in Nav1.3 null mutant mice. *Molecular pain* **2,** 33.

Nassar MA, Stirling LC, Forlani G, Baker MD, Matthews EA, Dickenson AH & Wood JN. (2004). Nociceptor-specific gene deletion reveals a major role for Nav1.7 (PN1) in acute and inflammatory pain. *Proc Natl Acad Sci U S A* **101,** 12706-12711.

Olivos L & Artalejo AR. (2007). Muscarinic excitation-secretion coupling in chromaffin cells. *Acta physiologica (Oxford, England)* **192,** 213-220.

Raman IM & Bean BP. (1997). Resurgent sodium current and action potential formation in dissociated cerebellar Purkinje neurons. *The Journal of neuroscience : the official journal of the Society for Neuroscience* **17,** 4517-4526.

Ritchie AK. (1979). Catecholamine secretion in a rat pheochromocytoma cell line: two pathways for calcium entry. *The Journal of physiology* **286,** 541-561.

Rush AM, Dib-Hajj SD & Waxman SG. (2005). Electrophysiological properties of two axonal sodium channels, Nav1.2 and Nav1.6, expressed in mouse spinal sensory neurones. *The Journal of physiology* **564,** 803-815.

Sangameswaran L, Fish LM, Koch BD, Rabert DK, Delgado SG, Ilnicka M, Jakeman LB, Novakovic S, Wong K, Sze P, Tzoumaka E, Stewart GR, Herman RC, Chan H, Eglen RM & Hunter JC. (1997). A novel tetrodotoxin-sensitive, voltage-gated sodium channel expressed in rat and human dorsal root ganglia. *The Journal of biological chemistry* **272,** 14805-14809.

Smith MR, Smith RD, Plummer NW, Meisler MH & Goldin AL. (1998). Functional analysis of the mouse Scn8a sodium channel. *The Journal of neuroscience : the official journal of the Society for Neuroscience* **18,** 6093-6102.

Swensen AM & Bean BP. (2003). Ionic mechanisms of burst firing in dissociated Purkinje neurons. *The Journal of neuroscience : the official journal of the Society for Neuroscience* **23,** 9650-9663.

Taddese A & Bean BP. (2002). Subthreshold sodium current from rapidly inactivating sodium channels drives spontaneous firing of tuberomammillary neurons. *Neuron* **33,** 587-600.

Toledo-Aral JJ, Moss BL, He ZJ, Koszowski AG, Whisenand T, Levinson SR, Wolf JJ, Silos-Santiago I, Halegoua S & Mandel G. (1997). Identification of PN1, a predominant voltage-dependent sodium channel expressed principally in peripheral neurons. *Proc Natl Acad Sci U S A* **94,** 1527-1532.

Tucker KR, Huertas MA, Horn JP, Canavier CC & Levitan ES. (2012). Pacemaker rate and depolarization block in nigral dopamine neurons: a somatic sodium channel balancing act. *J Neurosci* **32,** 14519-14531.

Vandael DH, Marcantoni A, Mahapatra S, Caro A, Ruth P, Zuccotti A, Knipper M & Carbone E. (2010). Ca(v)1.3 and BK channels for timing and regulating cell firing. *Molecular neurobiology* **42,** 185-198.

Vandael DHF, Zuccotti A, Striessnig J & Carbone E. (2012). Ca(V)1.3-Driven SK Channel Activation Regulates Pacemaking and Spike Frequency Adaptation in Mouse Chromaffin Cells. *Journal of Neuroscience* **32,** 16345-16359.

Wada A, Wanke E, Gullo F & Schiavon E. (2008). Voltage-dependent Na(v)1.7 sodium channels: multiple roles in adrenal chromaffin cells and peripheral nervous system. *Acta physiologica (Oxford, England)* **192,** 221-231.

Wakade AR. (1981). Studies on secretion of catecholamines evoked by acetylcholine or transmural stimulation of the rat adrenal gland. *The Journal of physiology* **313,** 463-480.

Wallace DJ, Chen C & Marley PD. (2002). Histamine promotes excitability in bovine adrenal chromaffin cells by inhibiting an M-current. *The Journal of physiology* **540,** 921-939.

Yanagita T, Satoh S, Uezono Y, Matsuo K, Nemoto T, Maruta T, Yoshikawa N, Iwakiri T, Minami K & Murakami M. (2011). Transcriptional up-regulation of cell surface Na V 1.7 sodium channels by insulin-like growth factor-1 via inhibition of glycogen synthase kinase-3beta in adrenal chromaffin cells: enhancement of 22Na+ influx, 45Ca2+ influx and catecholamine secretion. *Neuropharmacology* **61,** 1265-1274.

Zhou Z & Misler S. (1995). Action potential-induced quantal secretion of catecholamines from rat adrenal chromaffin cells. *The Journal of biological chemistry* **270,** 3498-3505.

Competing interests: All authors declare no conflict of interest.

Author contributions

D.H.F.V. contributed to data collection of whole-cell, single channel and amperometric experiments. M.M.O. and A.A. contributed to data collection of part of the whole-cell recordings. V.C. contributed to the design, analysis and interpretation of amperometric measurements. Ch.L., Cl.L. and N.C.G. contributed to the design, collection, analysis and interpretation of the qRT-PCR and immunoblotting. D.H.F.V. and E.C. contributed to the conception and design of the experiments, data analysis, drafting the article as well as revising it critically for important intellectual content with the input of all co-authors. All authors have approved the final version of the manuscript.

Fundings

This work was supported by the Italian MIUR (PRIN 2010/2011 project 2010JFYFY2) and the University of Torino.

Acknowledgments

We thank Dr. C. Franchino, L. Grimaud and B. Toutain for technical assistance.

Table 1 - Sequence of primers used for real-time RT-PCR

gene name	GenBank accession number	protein name	forward primer (5'-3')	reverse primer (5'-3')
scn1A	NM_018733.2	Nav1.1	ttgcaaggggcttctgttta	aggtccacaaactccgtcac
scn2A	NM_001099298.2	Nav1.2	gggttgcatatggtttccaa	cccaaggcatttgcagtta
scn3A	NM_018732.3	Nav1.3	tcctcagtagtggtgctttgg	gatgtaagtgaagactttgtcagca
scn4A	NM_133199.2	Nav1.4	gaaaaccatcacggtcatcc	tccgagagctttttcacagac
scn5A	NM_021544.4	Nav1.5	gccagatctctatggcaacc	ttgcccttattcagcacgat
scn8A	NM_001077499.2	Nav1.6	ctggtgctggttggacttc	gcccagggcattagctataa
scn9A	NM_018852.2	Nav1.7	aaagcaggtgggacaaagg	ctctccttggcactctttgag
scn10a	NM_009134.3	Nav1.8	gctgagcctatcaatgcaga	acttggcagcatggaaatct
scn11A	NM_011887.3	Nav1.9	tgggtagcttatggcttcaaa	ctatgaggcttgtgagggaga
scn1B	NM_011322.2	*β1*	tgctacaagaagattgctgctg	aatggccaggtattctgagg
scn2B	NM_001014761.2	*β2*	caggagtgtaacaattgcacaga	gggttccctgagaactccac
scn3B	NM_153522.2	*β3*	cccctagcttctctagtgctca	ctgtctccgagggtacttctaca
scn4B	NM_001013390.2	*β4*	tgaagaagacccgagagaaga	acccgttctctgtgttgtca
Gusb	NM_010368.1	Gus	ctctggtggccttacctgat	cagttgttgtcaccttcacctc
Hprt	NM_013556.2	Hprt	aggacctctcgaagtgt	attcaaatccctgaagtactcat
Gapdh	NM_008084.2	Gapdh	ccggggctggcattgctctc	ggggtgggtggtccagggtt

Figure legends

Fig 1. *Expression profile of Nav channel α and β-subunit genes and immunodetection of Nav1.3 and Nav1.7 proteins in the mouse adrenal medulla*. **a**, RT-qPCR data illustrating that among all Nav channel genes, only TTX-sensitive isoforms are expressed in adrenal medulla with a major expression for mRNAs encoding Nav1.3 and Nav1.7 (left histogram, ***p<0.001 for scn3a compared to scn9a). Except for scn4b (β4-subunit) all β-subunit mRNAs are present (right histogram, **p<0.01 for scn3b compared to scn1b). Significance tests between groups of data were performed using one-way ANOVA followed by a Bonferroni post hoc test. Data are mean ± s.e.m. of 6 independent samples. **b**, western blot analysis of proteins extracted from macrodissected mouse adrenal medulla (am, 10 µg) and from mouse brain (b, 30 µg). Note that 3-fold higher amount of proteins was used for the brain, due to the weak expression of Nav1.3 and Nav1.7 channels, as reported (Sangameswaran *et al.*, 1997; Catterall *et al.*, 2005). When probed for Nav1.3 and Nav1.7 proteins, a single band is immunodetected at 230 kDa (Nav1.3) and 220 kDa (Nav1.7) in both tissues, with stronger signal intensities in the adrenal medulla (upper membranes). Immunoblotting of β-actin was used as a control (lower membranes).

Fig 2. *Nav channels in MCCs are transient and fully blocked by TTX*. **a.** TTX dose-response curve representing the mean of 11 cells, fitted by a sigmoidal function with IC_{50} = 7 nM. Traces are normalized against control values. Currents were triggered by step depolarizations to -10 mV from V_h -70 mV every 5 s. **b.** Whole cell Nav currents after subtraction of TTX-insensitive currents evoked by 1 s lasting depolarizing pulses in steps of 10 mV from V_h -70 mV (n =8). The left inset shows the transient segment of Nav currents at a more expanded time scale. The right inset shows an enlargement of the current at steady-state indicated by the arrow. The bottom inset shows the I/V relationship for the transient component (continuous line) and the steady state component (dotted line). **c.** Three representative single channel traces recorded from perforated microvesicles pulled off from 6 MCCs at -20, -30 and -40 mV. Bottom trace represents the ensemble currents obtained by summing-up 10 consecutive single channel traces. Decay of the ensemble currents were fitted by a single exponential function (grey line superimposing the current trace). Grey windows show ensemble currents at steady-state indicated by the arrow. **d.** single channel slope conductance obtained by linear fit through the mean unitary current amplitudes estimated within the last 800 ms of the recording at -40 mV (226 openings), -30 mV (243 openings) and -20 mV (111 openings). **e.** Time constants of Nav current inactivation for whole-cell currents (referred to **b**, thick line) and ensemble currents (referred to **c**, dotted line) obtained from single exponential fits. **f.** single channel mean dwell times for the indicated potentials, starting at V_h -70 mV. **g.** estimated mean open probability of Nav channels during the

steady state normalized to the total amount of channels in the patch. **h**. Single channel traces obtained at the indicated test potentials at expanded time scale (100 ms).

Fig 3. *Holding potential dependent availability of MCC Nav channels and window currents.* **a.** Representative Nav currents evoked from varying V_h as indicated: -100 mV (black), -80 mV (red), -60 mV (blue), -40 mV (green). Cells were kept for 10 s at V_h before recording; intersweep intervals of 5 s were applied. Traces shown were obtained after subtracting the TTX-insensitive current traces measured in the presence of 300 nM TTX. **b.** I-V relationship (n = 26) for Nav current densities measured at the indicated V_h. **c.** Normalized conductance (n = 26) (derived from the data shown in **b**) and normalized steady state inactivation (n = 16) measured at -10 mV for the indicated V_h. Boltzmann equations were used for fitting both activation and inactivation curves. Insets depict representative traces that show steady state inactivation of Nav currents at the indicated V_h. Half-maximal values (in mV) and slope factors of activation (in mV) obtained from the fit are -21.9 and 5.5 for V_h = -100 mV; -21.3 and 5.0 for, -80 mV, 20.3 and 5.5 for -60 mV, -13.4 and 6.0 for -40 mV, respectively. Half maximal inactivation (in mV) and slope factors of inactivation (in mV) are -44.6 and 7.6 at V_h = -100 mV, -46.0 and 8.2 at -80 mV, -48.0 and 9.5 at -60 mV, -59.7 and 13.4 at -40 mV, respectively.

Fig 4. *Holding potential dependent reduction of window currents and channel availability in MCCs.* **a.** top panels show whole-cell currents; middle panels show open probabilities (P_o) obtained by multiplying activation and inactivation curves shown in Fig. 3c; bottom panels show the window currents calculated by multiplying the whole-cell currents (top) by P_o (middle). The V_h of the experiment are indicated on top: -100 mV (black), -80 mV (red), -60 mV(blue) and -40 mV (green). **b.** availability of Nav current densities with respect to the indicated holding potentials (n = 26). Data were fit by a Boltzmann equation. The half maximal value and slope factor of inactivation are -47.9 mV and 10.5 mV. **c.** overlap of activation and inactivation curves at V_h -100 mV (black) and V_h -40 mV (green), derived from Fig. 3.

Fig 5. *Inactivation properties of MCC Nav channels*. **a.** recovery from steady state inactivation of Nav currents from V_h = -90 mV (blue, n = 13), -50 mV (black, n = 14) and -40 mV (red, n = 10). Current amplitudes at the test pulse (I_2) were normalized against current amplitudes at the preceding pulse (I_1). Averaged data were fit by double exponentials with fast and slow components of different amplitude (A_{fast}, A_{slow}) and time constants (τ_{fast}, τ_{slow}). τ_{fast}, τ_{slow} and amplitudes (in parenthesis) were: 4.8 ms (0.6) and 156 ms (0.4) at -90 mV, 21.3 ms (0.6) and 501 ms (0.3) at -50 mV, 23.7 ms (0,34) and 229 ms (0.22) at -40 mV. **b.** On-set of closed-state slow inactivation during V_h = -90 mV (blue, n = 10), -50 mV (black, n = 5) and -40 mV (red, n = 6). Current amplitudes during the test pulse (I_2) were compared with currents at onset (I_1). The

conditioning pulse was followed by a recovery period of 1.2 s in order to allow recovery from fast inactivation. Data were fit by a single exponential function of different time constant (τ) and amplitude (A). τ and A (in parenthesis) were 7.8 s (0.32) at V_h = -90 mV, 1.6 s (0.45) at -50 mV and 0.58 s (0.54) at -40 mV. **c.** Nav and L-type currents elicited by ramp depolarizations starting from V_h -50 mV (black) or V_h -40 mV (red). Nav currents are the result of subtracting control traces from the TTX-resistant component. L-type currents (blue) are the results of subtracting control traces from nifedipine-insensitive currents. Inset to the right are mean ± SEM of peak Na^+ and L-type currents at different ramp duration. **d.** comparison of Nav currents evoked by a 20 ms ramp in the presence (I_2, red trace) or absence (I_1, black trace) of a preceding slow pacemaker like ramp of 1 s duration following the indicated protocol on top (***p 0.001, paired Student's t test). The black and red voltage-clamp protocols indicated on top were separated in time by 5 s. The starting voltage of the ramp (-55 mV) is the mean AHP peak of the APs while -28 mV is the mean spike threshold value (see Vandael et al., 2012).

Fig 6. *Chromaffin cell stimulation leads to Nav channel inactivation and AP widening*. **a.** representative response of a current clamped MCC to a 10 mV steady depolarization. The right panel shows the overlap of a control AP (black) with an AP obtained after the imposed depolarization (grey). **b.** Phase plane plots (*dV/dt* vs *V*) from the same cell constructed by averaging n= 4 APs at V_h= -50 and n= 5 APs at -40 mV, respectively. To the right are the effects of a 10 mV depolarization on spike parameters (***p 0.001, paired Student's t-test). Half width was measured as the duration of the AP at half of the total amplitude (from the after-hyperpolarization peak to overshoot peak). **c.** Nav currents measured by AP-clamp using APs at rest (left) and APs that originate from a depolarized resting potential (right). Middle panel shows control trace in black and TTX (300 nM) resistant component in grey. Bottom panel shows the pure Nav currents after subtraction for TTX-insensitive currents. Top-right inset shows normalized current amplitudes against the first current peak amplitude of the spike train. The grey line and dots refer to Nav currents triggered at depolarized resting potentials (-40 mV, n= 12) while the black line and squares represent Nav currents that flow during spikes at rest (n = 12) (*p 0.05, ***p<0.001, paired Student's t-test). Bottom-right inset represents the ratio between Nav currents triggered by control APs and APs at depolarized resting potentials for each consecutive spike (*p 0.05, ANOVA followed by a Bonferroni *post hoc* analysis).

Fig 7. *TTX leads to a dose dependent switch into burst firing of MCCs*. **a.** representative current clamp trace showing the action of increasing TTX concentration. **b.** top gives a better view of the effects of diverse TTX concentrations on the AP waveforms and firing patterns at slower and faster (grey windows) time scales. Periods of activity were taken from panel **a**. Middle panel illustrates the interspike interval duration (ISI) distribution for the indicated TTX concentrations.

Lower panel shows joint interspike interval plots obtained by plotting each ISI on the x-axis (ISI_i) against its succeeding ISI duration (ISI_{i+1}) on the y-axis. Random firing in the absence or presence of 10 nM TTX leads to a cloudy pattern while burst firing patterns at elevated TTX concentration (30 to 300 nM) leads to an L-shaped distribution. **c.** dose response curve of AP peak vs. TTX concentration. Data were fit with a sigmoid function with saturating value at 17.5 mV (IC_{50} = 9 nM). **d**. dose response curve of AP half-width vs. TTX concentration. Data were fit with a sigmoid function with saturating value at 26.2 ms (IC_{50} = 18.7 nM). **e.** dose response curve of the fraction of spikes fired in bursts vs. TTX concentration. Data were fit with a sigmoid function with saturating value at 76% (IC_{50} = 39.9 nM).

Fig 8*. Reducing Na_V availability inverts net current covering the AHP from outward to inward*. **a**. (top) AP-clamp experiment showing representative ctrl spike. (middle) K_v currents (red traces) were measured in a Tyrode standard solution with TTX (300 nM) and Cd^{2+} (200 μM). Ca^{2+} currents (black) were measured in the presence of TTX (300 nM) and high extracellular TEA (135 mM). Ca^{2+}-activated K^+ currents (blue) were obtained by subtracting from a control recording in tyrode standard with TTX (300 nM) the K_V and the Ca^{2+} current. (bottom) close up of the middle panel. The grey rectangle indicates the AHP phase and the respective currents that sustain it. **b, c.** same as for **a**, using a single spike stimulus protocol triggered from -40 mV and a spike doublet fired after complete block of Nav currents with 300 nM TTX. Inset in **b:** net current amplitudes measured during the AHP phase indicated by the grey windows. Inset in **c**: Ca^{2+} charge entering the cell during the AHP phase calculated by the integrating the corresponding Ca^{2+} inward current (*p<0.05; ***p<0.001; n = 9; ANOVA followed by a Bonferroni *post hoc* analysis).

Fig. 9*. Spontaneous burst firing in a minority of MCCs*. **a**. left, representative trace of spontaneous trains of APs fired in burst-like mode. Center: a single burst at an expanded time scale. Right: overlap of consecutive APs of a burst. Numbers indicate the position/sequence in the burst. **b.** evolution of the AP peak, AHP amplitude, half width, interspike interval and instantaneous firing frequency of consecutive spikes in a burst. Mean values were obtained for each bursting cell (n= 39) and then averaged. **c**. AP-clamp experiment measuring K_V (n= 18) and BK (n= 7) currents. Top shows the burst recorded and used as voltage command (black trace), K_V currents are shown in red and BK currents in grey. **d-e.** as for **c** but currents isolated were Ca^{2+} (blue, n= 17), SK (orange, n= 7) and Na^+ (black, n= 6). **f.** top, BK, SK and Kv outward current amplitudes versus the spike number of the burst. Bottom, same as top but for the Na^+ and Ca^{2+} inward currents (***p<0.001, paired Student's t test).

Fig 10*. Burst firing associated with Nav channel block boosts MCC exocytosis*. **a.** example of combined recording of APs (black traces) and amperometric events (grey traces) by carbon fiber

amperometry in control. **b.** representation of combined recording of AP bursts after TTX application (same cell as shown in **a**) and amperometric events by amperometry. **c.** overlap of cumulative secretion plots obtained from amperometric measurements shown in **a** and **b** for control (black curve) and during TTX application (grey curve). **d**. comparison of amperometric spike parameters (see top panel), frequency and cumulative charge between control (black bars) and TTX-treated cells (grey bars) (*$p<0.05$ and **$p<0.01$, n= 14; paired Student's t test).

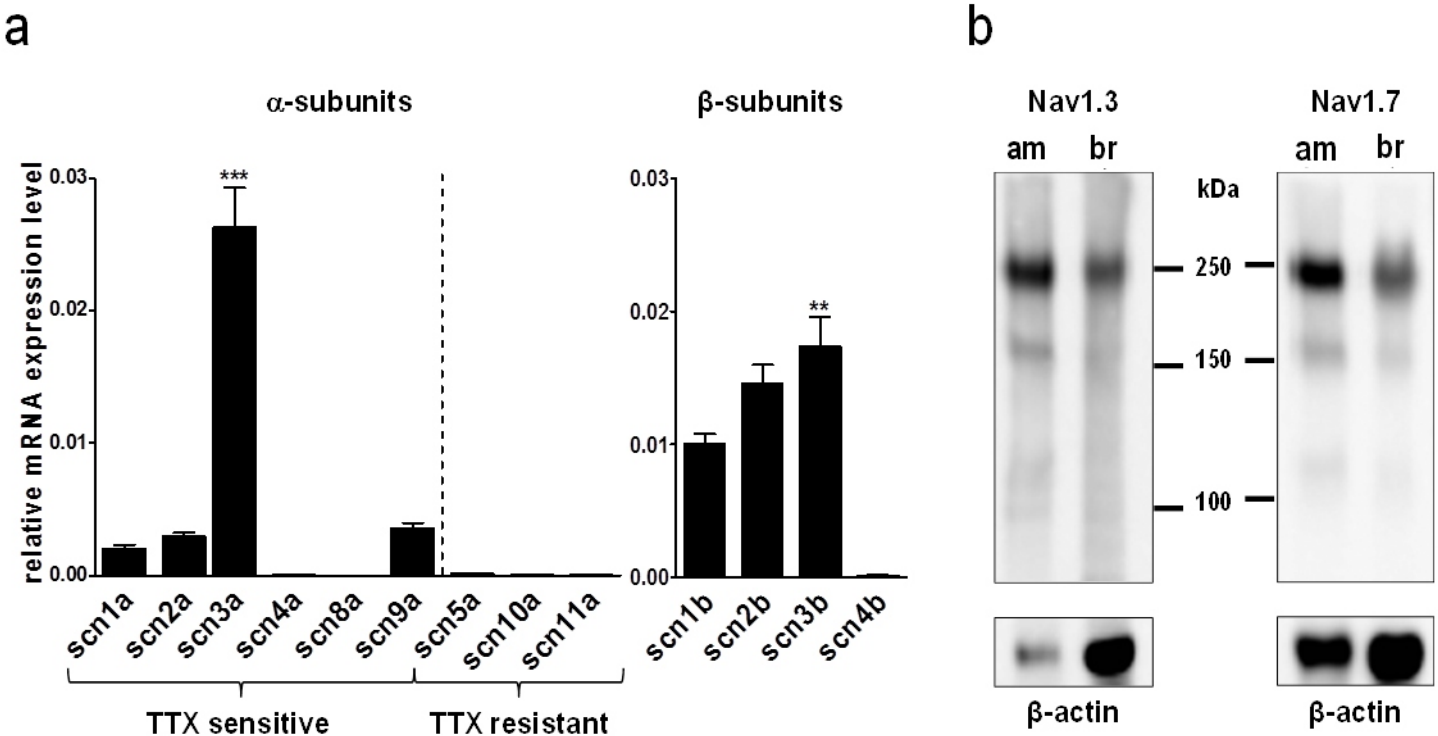
a
α-subunits
β-subunits
relative mRNA expression level
0.03
0.02
0.01
0.00
***
**
scn1a
scn2a
scn3a
scn4a
scn8a
scn9a
scn5a
scn10a
scn11a
scn1b
scn2b
scn3b
scn4b
TTX sensitive
TTX resistant
b
Nav1.3
Nav1.7
am
br
kDa
250
150
100
β-actin

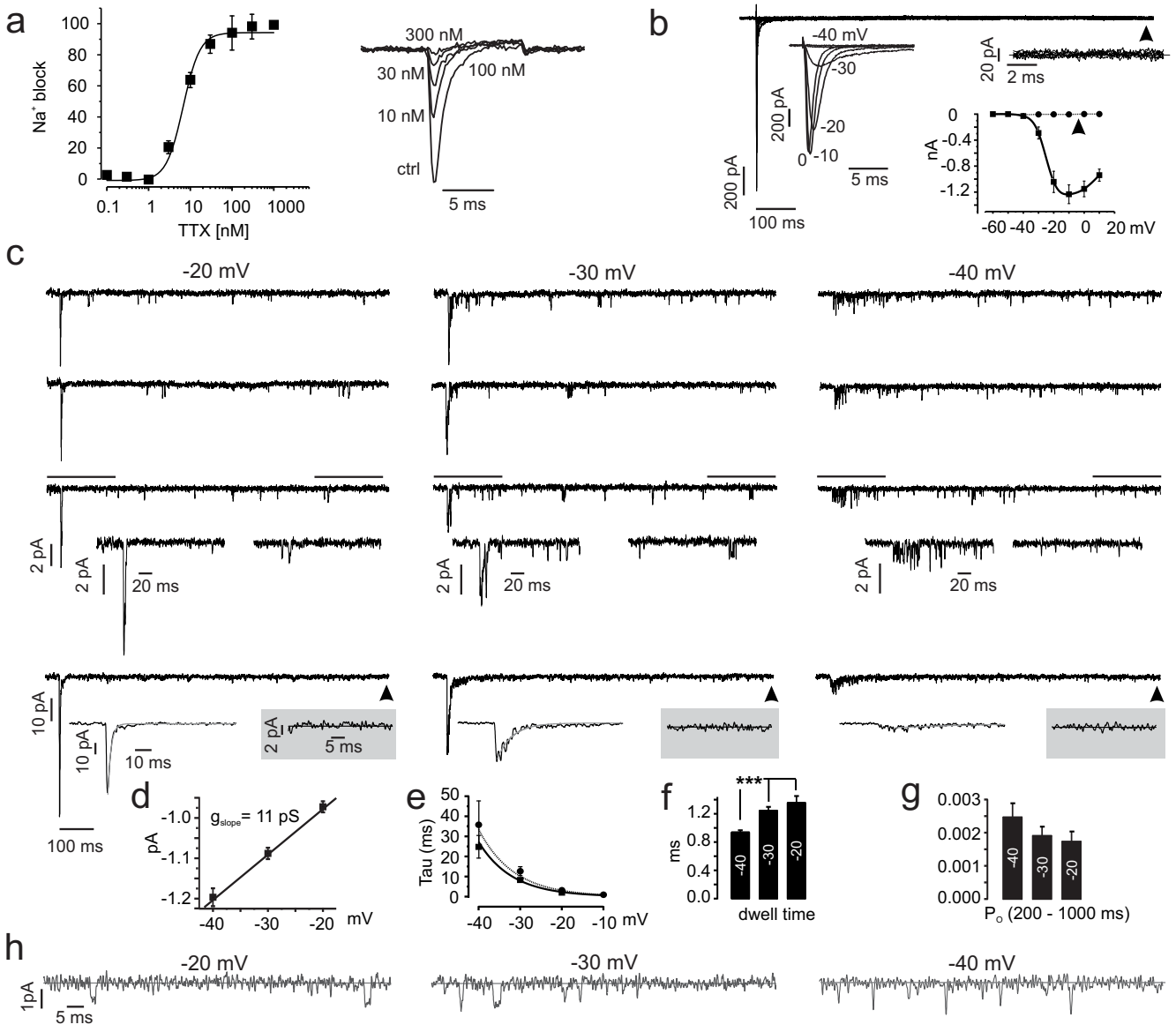
a
Na+ block
TTX [nM]
300 nM
30 nM
100 nM
10 nM
ctrl
5 ms
b
-40 mV
-30
-20
-10
200 pA
5 ms
100 ms
20 pA
2 ms
nA
20 mV
c
-20 mV
-30 mV
-40 mV
2 pA
20 ms
10 pA
10 ms
5 ms
100 ms
d
g_slope = 11 pS
pA
mV
e
Tau (ms)
f
***
ms
dwell time
g
P_o (200 - 1000 ms)
h
1pA
5 ms

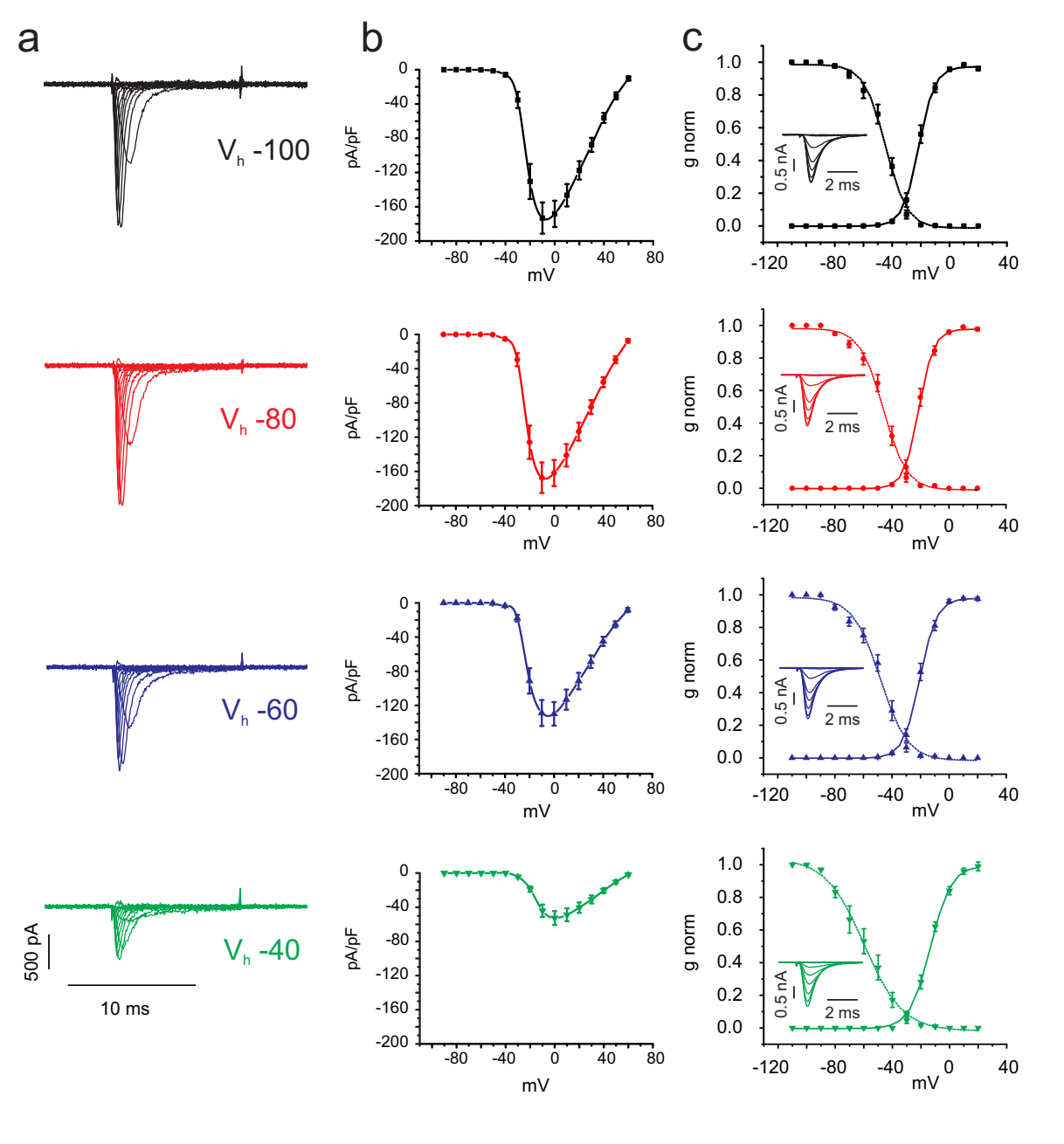
a
b
c
V_h -100
V_h -80
V_h -60
V_h -40
500 pA
10 ms
pA/pF
mV
g norm
0.5 nA
2 ms

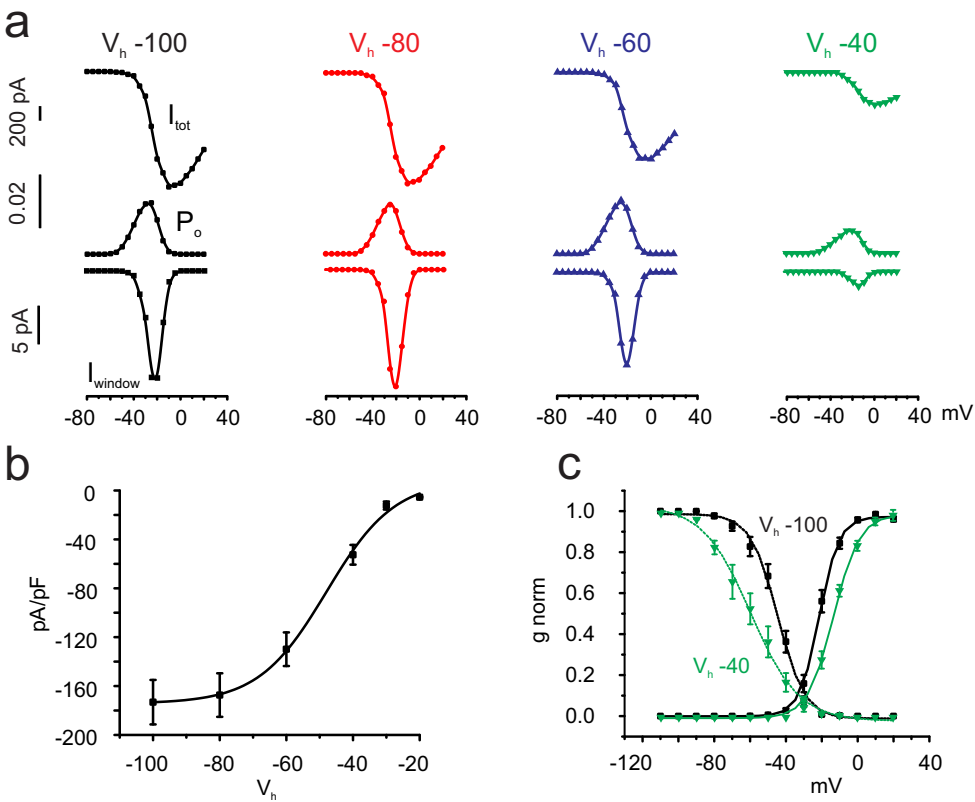
a
V_h -100
V_h -80
V_h -60
V_h -40
200 pA
0.02
5 pA
I_tot
P_o
I_window
-80 -40 0 40
mV
b
pA/pF
0
-40
-80
-120
-160
-200
-100 -80 -60 -40 -20
V_h
c
g norm
1.0
0.8
0.6
0.4
0.2
0.0
V_h -100
V_h -40
-120 -80 -40 0 40
mV

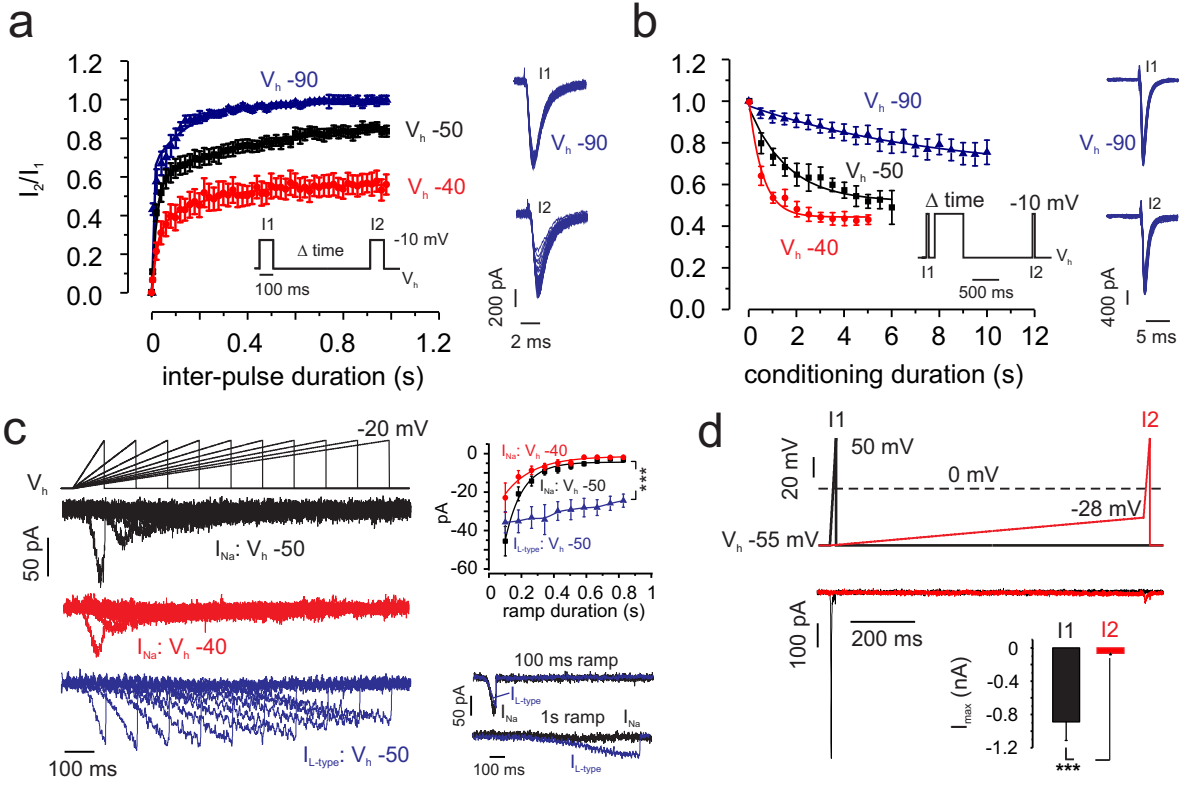
a
1.2
1.0
0.8
0.6
0.4
0.2
0.0
I2/I1
V_h -90
V_h -50
V_h -40
I1
I2
Δ time
-10 mV
100 ms
V_h
0
0.4
0.8
1.2
inter-pulse duration (s)
I1
V_h -90
I2
200 pA
2 ms
b
1.2
1.0
0.8
0.6
0.4
0.2
0.0
V_h -90
V_h -50
V_h -40
Δ time
-10 mV
I1
I2
500 ms
V_h
0
2
4
6
8
10
12
conditioning duration (s)
I1
V_h -90
I2
400 pA
5 ms
c
-20 mV
V_h
50 pA
I_Na: V_h -50
I_Na: V_h -40
100 ms
I_L-type: V_h -50
I_Na: V_h -40
I_Na: V_h -50
I_L-type: V_h -50
***
0
-20
-40
-60
pA
0
0.2
0.4
0.6
0.8
1
ramp duration (s)
100 ms ramp
50 pA
I_L-type
I_Na
1s ramp
I_Na
100 ms
I_L-type
d
I1
I2
20 mV
I
50 mV
0 mV
-28 mV
V_h -55 mV
100 pA
200 ms
I1
I2
0
-0.4
-0.8
-1.2
I_max (nA)
***

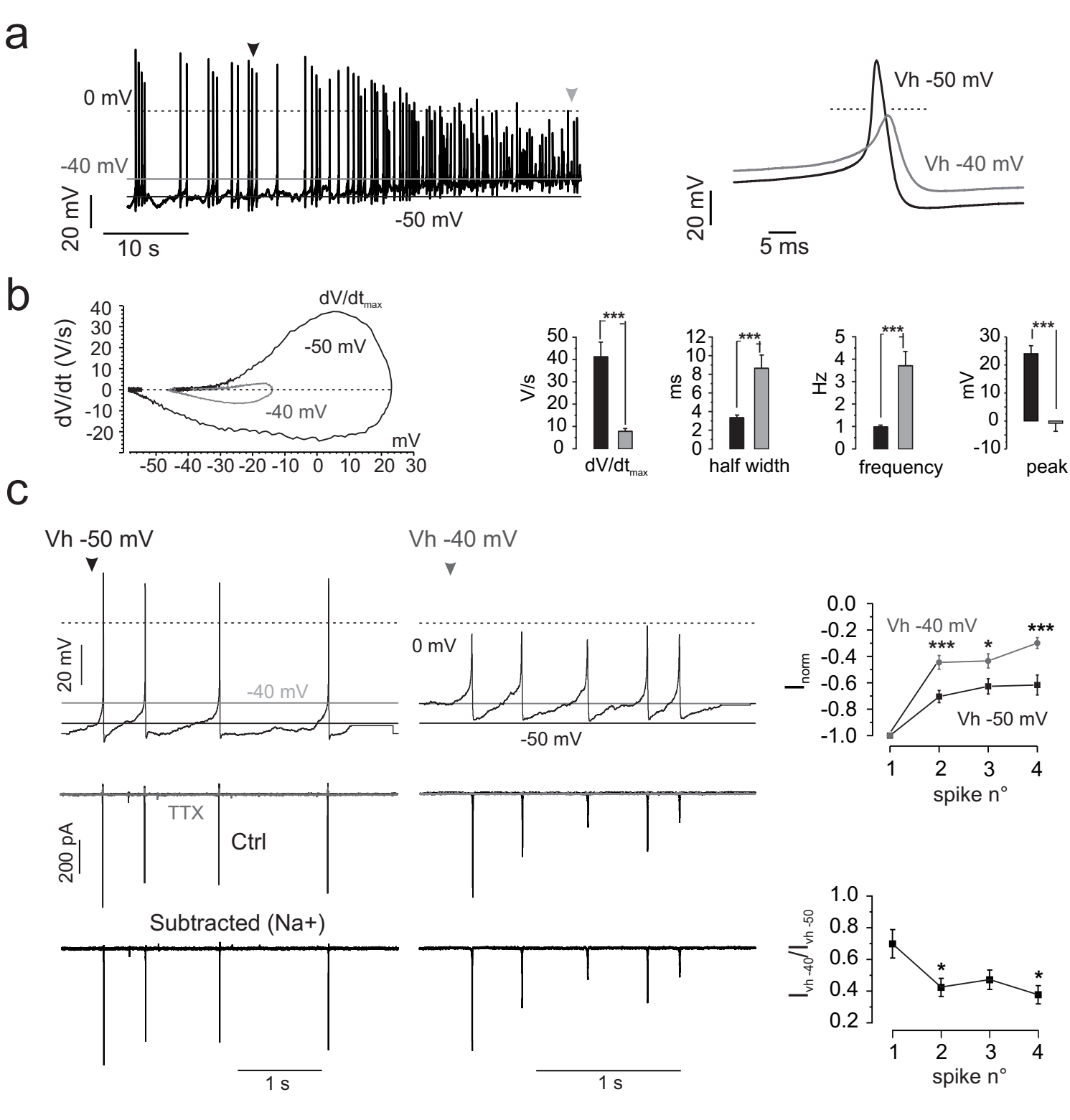
a
0 mV
-40 mV
20 mV
10 s
-50 mV
Vh -50 mV
Vh -40 mV
20 mV
5 ms
b
dV/dt (V/s)
dV/dt$_{max}$
-50 mV
-40 mV
mV
V/s
dV/dt$_{max}$
ms
half width
Hz
frequency
mV
peak
***
c
Vh -50 mV
Vh -40 mV
20 mV
-40 mV
0 mV
-50 mV
200 pA
TTX
Ctrl
Subtracted (Na+)
1 s
1 s
I$_{norm}$
Vh -40 mV
Vh -50 mV
spike n°
I$_{vh-40}$/I$_{vh-50}$
spike n°
*
***

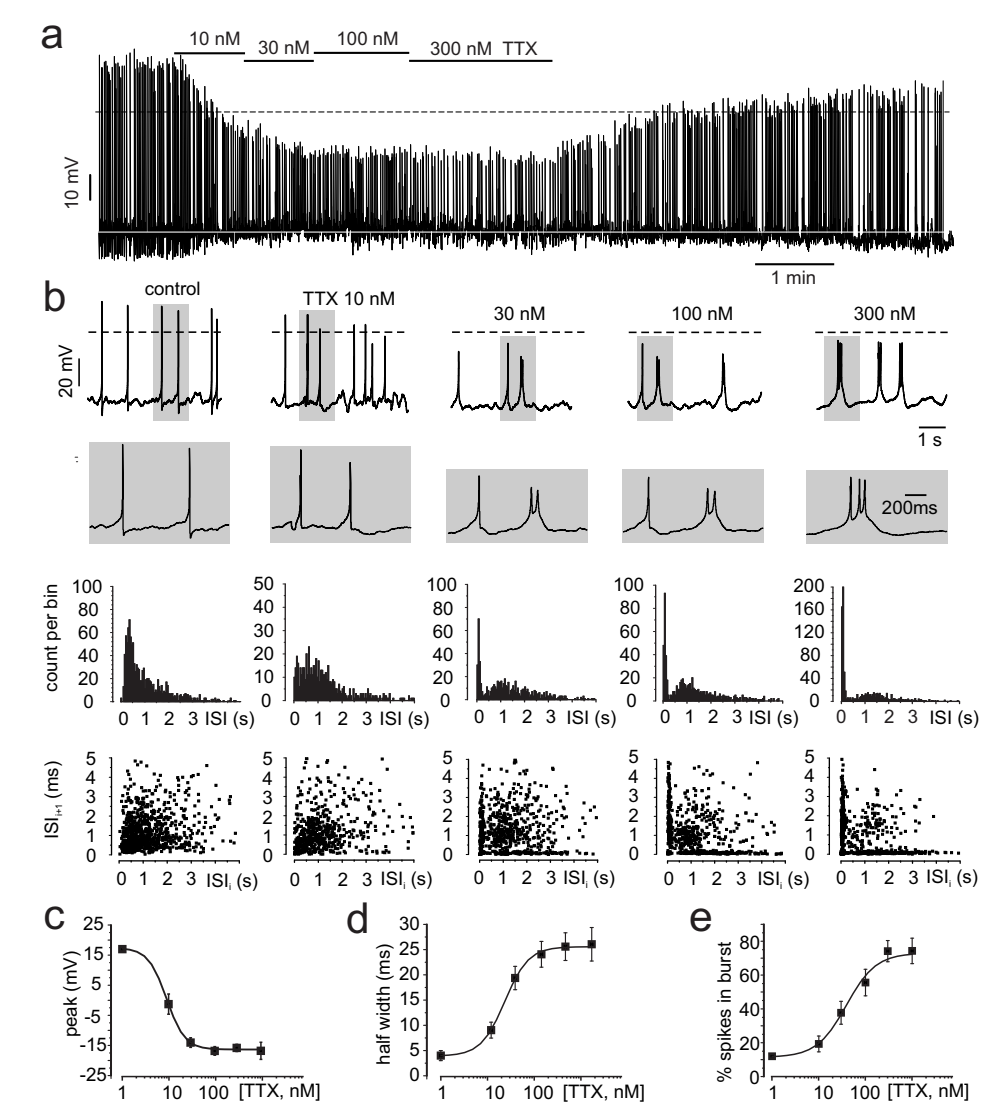
a
10 nM
30 nM
100 nM
300 nM TTX
10 mV
1 min
b
control
TTX 10 nM
30 nM
100 nM
300 nM
20 mV
1 s
200ms
count per bin
ISI (s)
ISI$_{i+1}$ (ms)
ISI$_i$ (s)
c
peak (mV)
[TTX, nM]
d
half width (ms)
[TTX, nM]
e
% spikes in burst
[TTX, nM]

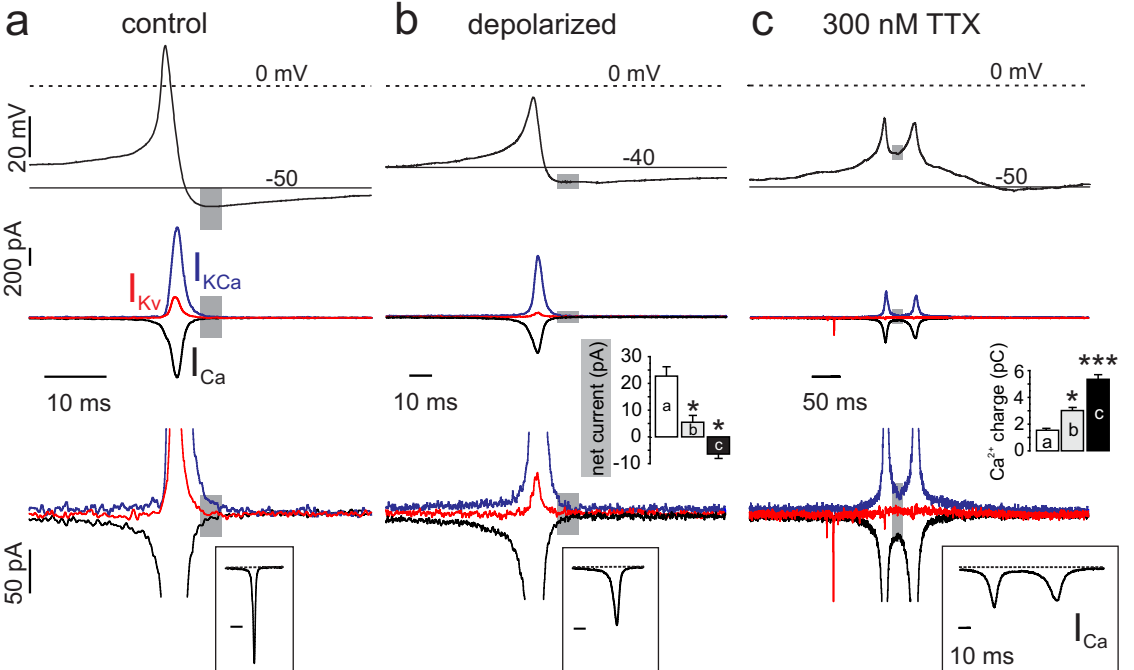
a
control
b
depolarized
c
300 nM TTX
0 mV
20 mV
-50
-40
200 pA
I_Kv
I_KCa
I_Ca
10 ms
50 ms
net current (pA)
Ca2+ charge (pC)
50 pA
10 ms

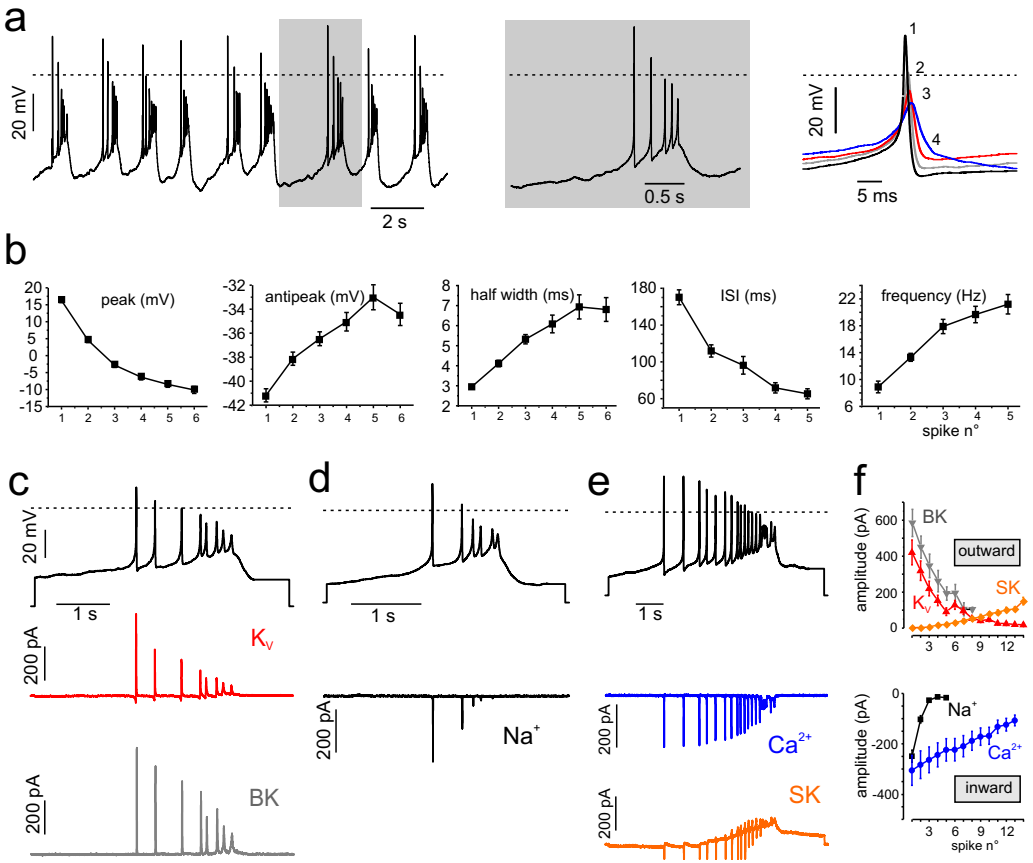
a
20 mV
2 s
0.5 s
1
2
3
4
20 mV
5 ms
b
peak (mV)
antipeak (mV)
half width (ms)
ISI (ms)
frequency (Hz)
spike n°
c
20 mV
1 s
200 pA
K_v
200 pA
BK
d
1 s
200 pA
Na^+
e
1 s
200 pA
Ca^{2+}
200 pA
SK
f
amplitude (pA)
BK
outward
SK
K_v
amplitude (pA)
Na^+
Ca^{2+}
inward
spike n°

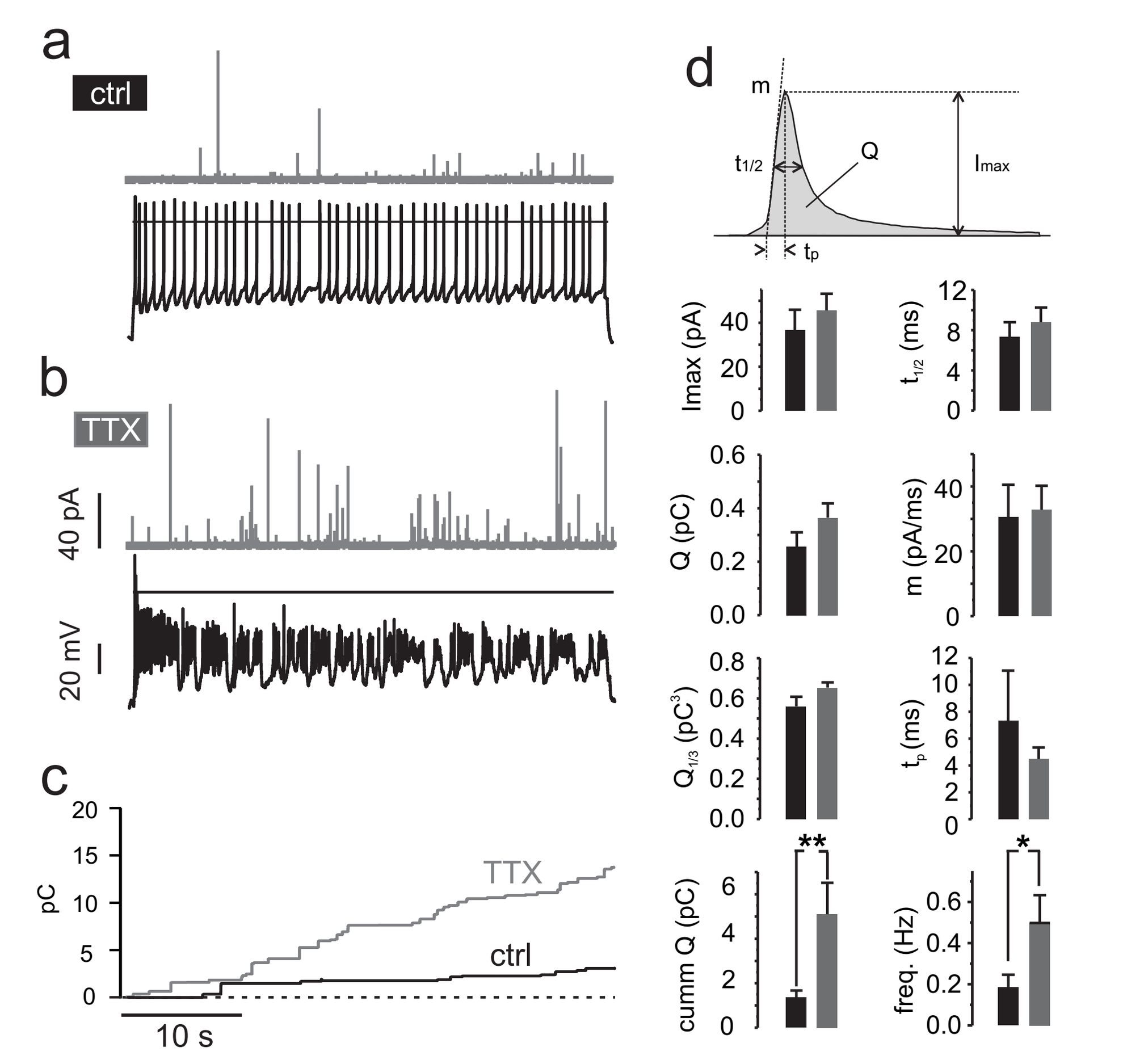
a
ctrl
b
TTX
40 pA
20 mV
c
pC
20
15
10
5
0
TTX
ctrl
10 s
d
m
t1/2
Q
Imax
tp
Imax (pA)
40
20
0
t1/2 (ms)
12
8
4
0
Q (pC)
0.6
0.4
0.2
0.0
m (pA/ms)
40
20
0
Q1/3 (pC3)
0.8
0.6
0.4
0.2
0.0
tp (ms)
12
10
8
6
4
2
0
cumm Q (pC)
6
4
2
0
**
freq. (Hz)
0.6
0.4
0.2
0.0
*